The following publication Xu, J., & Liu, Z. (2021). The First Validation of Sentinel-3 OLCI Integrated Water Vapor Products Using Reference GPS Data in Mainland China. IEEE Transactions on Geoscience and Remote Sensing, 60, 1-17 is available at https://doi.org/10.1109/TGRS.2021.3099168.

# The First Validation of Sentinel-3 OLCI Integrated Water Vapor Products Using Reference GPS Data in Mainland China

Jiafei Xu, and Zhizhao Liu

***Abstract*—The integrated water vapor (IWV) products collected during June 1, 2019 to May 31, 2020 from the Ocean and Land Color Instrument (OLCI) sensor, on board the Sentinel-3 satellites, are evaluated against reference water vapor data estimated from ground-based 214 Global Positioning System (GPS) stations in the Mainland China. This is the first time to thoroughly evaluate the quality of Sentinel-3 OLCI IWV products by in-situ GPS-measured IWV data from such a large spatial coverage as China. The validation results show that, under cloud-free conditions, the OLCI IWV measurements agree very well with the ground-based GPS water vapor data, with a root-mean-square error (RMSE) of 3.03 mm for Sentinel-3A satellite and 3.13 mm for Sentinel-3B satellite. The dependence of OLCI IWV on various parameters was also analyzed. Analysis showed that the accuracy of inland OLCI IWV products was superior to that in coastal areas and that OLCI tended to overestimate IWV value in lower elevation and underestimate IWV value in higher elevation. The accuracy of OLCI IWV measurements increased as IWV decreased. Solar zenith angle analysis showed that the OLCI IWV product had a higher accuracy at a larger solar zenith angle. In spring and winter, the OLCI IWV observations had higher accuracy than those in summer and autumn. OLCI IWV tended to underestimate IWV value in most land cover types. Except for the polar climatic zone, the Sentinel-3 OLCI IWV products tended to overestimate IWV value. The validation results against previous studies were also discussed in this work.**

***Index Terms*— GPS, integrated water vapor (IWV), Ocean and Land Color Instrument (OLCI), validation.**

## I. Introduction

Atmospheric water vapor is a key element in the climate system of Earth [1], which plays a significant role in affecting the hydrological cycle [2], [3], weather forecasting [4], and climate change [3], [5]. It usually has a high variability in the spatial and temporal domains [6], [7], and as a consequence, it has been declared an essential climate variable by the Global Climate Observing System (GCOS) [8]. Long time-series observation of water vapor in the atmosphere is of significant importance in the Earth's weather and climate system [5]. In order to develop accurate models to study local and global climate trends, it is essential to observe water vapor as accurately as possible.

Numerous measurement techniques have been developed to obtain water vapor information in the atmosphere, including space-based and ground-based observation techniques. Satellite remotely sensed measurements have been widely employed in observing integrated water vapor (IWV) in the atmosphere, because they can provide atmospheric water vapor observations at a global coverage [9], [10]. For IWV retrieval from different spectral bands of space-based satellite observation, four types of algorithms have been utilized: the microwave (MW) channel retrieval approach [11], [12], the infrared (IR) channel retrieval approach [13], [14], the near-infrared (NIR) channel retrieval approach [15]–[17], and the visible (VIS) channel approach [18], [19]. In addition to satellite-sensed IWV observations, many ground-based measurement networks have been established to observe atmospheric water vapor with a high temporal resolution, but only at each individual observation site. These in-situ techniques include microwave radiometers [20], [21], radiosondes [22], [23], sun photometers [24], [25], and Global Positioning System (GPS) [26]–[28]. Among the ground-based measurements, radiosonde and GPS are widely used as reference techniques to validate other satellite-sensed water vapor retrieval techniques [23], [29]–[31]. However radiosonde has low temporal resolution usually with two measurements per day [32]. Instead, GPS measurements can provide a high time resolution with dozens of records for both day time and nighttime [32].

Various studies have been conducted to evaluate the accuracy of satellite retrieved water vapor data, aiming to improve the understanding of the quality of satellite remotely sensed water vapor data. Vaquero-Martínez *et al.* [32] evaluated the accuracies of the IWV products derived from satellite measurements with ground-based GPS-sensed IWV observations at the Iberian Peninsula. The inter-comparison results suggested that, all satellite instruments tend to either underestimate high IWV or overestimate low IWV. He and Liu [33] utilized ground-based GPS water vapor measurements as a reference dataset to assess the retrieval accuracies of three typical NIR IWV products from Moderate Resolution Imaging Spectroradiometer (MODIS)/Terra, Medium Resolution Imaging Spectrometer (MERIS)/Envisat, and Medium Resolution Spectral Imager (MERSI)/FY-3A. Their findings indicated that the MERIS/Envisat has the highest IWV retrieval

This work was supported in part by the Key Program of the National Natural Science Foundation of China under Project 41730109, in part by the Hong Kong Research Grants Council (RGC) under Project Q73B PolyU 15211919, and in part by the Emerging Frontier Area (EFA) Scheme of Research Institute for Sustainable Urban Development (RISUD) of The Hong Kong Polytechnic University under Grant 1-BBWJ *(Corresponding author: Zhizhao Liu).*

The authors are with the Department of Land Surveying and Geo-Informatics, The Hong Kong Polytechnic University, Hong Kong, and also with the Research Institute for Sustainable Urban Development, The Hong Kong Polytechnic University, Hong Kong (e-mail: 20074506r@connect.polyu.hk; lszzliu@polyu.edu.hk).

accuracy with the smallest root-mean-square-error (RMSE) value of 3.708 mm under clear sky conditions in North America. Wang *et al*. [34] characterized the Ozone Monitoring Instrument (OMI) IWV products by comparing against commonly used reference datasets, such as GPS data over land and Special Sensor Microwave Imager/Sounder (SSMIS) data over the oceanic areas. It is clearly found that the overall mean between OMI IWV products and GPS measurements is 0.32 mm with a standard deviation of 5.2 mm over land; over the oceans, the overall mean between OMI and SSMIS IWV data is 0.40 mm with a standard deviation of 6.5 mm. Mertikas *et al*. [35] compared the IWV product estimated from Sentinel-3 OLCI data and IWV from GPS observations in Crete, Greece, illustrating that the bias between OLCI-retrieved IWV data and ground-based GPS-measured IWV data is -0.57±2.90 mm for Sentinel-3A and +2.42±3.41 mm for Sentinel-3B. These validations of satellite-derived IWV data were usually performed using the ground-based GPS IWV measurements as a reference [32]–[35].

The Sentinel-3A and Sentinel-3B were launched by the European Space Agency (ESA) on February 16, 2016, and April 25, 2018, respectively, to replace the Envisat satellite. One of the main aims of the Sentinel-3 mission is to measure Earth's weather and climate over land and ocean [36]. The OLCI instrument onboard the Sentinel-3 satellite is based on the proven heritage of Envisat's MERIS [37]. The OLCI sensor on board Sentinel-3A and Sentinel-3B has 21 spectral channels, whereas the predecessor MERIS instrument onboard Envisat had 15 bands only [37]. The Sentinel-3 OLCI sensors have provided operational Level-2 IWV products with a spatial resolution of 300 m over all target surfaces [38]. As one of the newest satellites, assessing the accuracies of the water vapor products is an important issue. However, few publications have reported the result of validating Sentinel-3 OLCI IWV products.

Previous evaluation of Sentinel-3 IWV products was only conducted over a limited area using a few ground-based GPS stations (i.e., 10 sites) [35]. Because atmospheric water vapor varies significantly in both spatial and temporal coverages [6], [7], it is hard to gain a reliable and comprehensive analysis of the Sentinel-3 water vapor retrieval accuracy with only a small spatial scale. To our best knowledge, there has been no publication related to the validation of Sentinel-3 OLCI IWV products in a large-spatial-scale area like China.

In this study, we conducted a comprehensive comparison analysis for Sentinel-3 OLCI IWV products at a large spatial coverage, i.e., China. The derived OLCI IWV data for the whole year between June 2019 and May 2020 were utilized to compare with GPS retrieved IWV data. Section II provided a detailed description of the data used in this study. The water vapor retrieval methodologies for ground-based and satellite-based measurements were presented in Section III. It also presented quantitative assessment approach used for assessing the accuracies of the derived OLCI IWV products. In Section IV, the comparison results between operational Sentinel-3 OLCI IWV products and GPS-measured IWV observations were analyzed and discussed. The Section V summarized the key conclusions.

## II. Data and Pre-Processing

The research area covers the interior and coastal areas of the Mainland China, with latitude from 16°42' N to 53°33' N and longitude from 73°40' E to 135°03' E (see Fig. 1). A total of 214 ground-based GPS sites were employed in this study. The type of land surface of these ground-based stations varies widely from arid areas to wet areas. The detailed information of the study area and the spatial distribution of in-situ GPS stations are displayed in Fig. 1. Two types of data sets were utilized in this comparison study, i.e. ground-based GPS-derived IWV measurements, and OLCI IWV products retrieved from Sentinel-3A and Sentinel-3B observations. Table I provides a summary of the characteristics of the data used in this research.

### *A. Ground-based IWV data*

The ground-based water vapor data used as reference in this study were calculated from the Crustal Movement Observation Network of China (CMONOC) observations [39], [40]. It has established a GPS network to provide continuous, full-weather, and full-time monitoring of atmospheric water vapor in China [39], [40]. The tropospheric zenith total delay (ZTD) products from the CMONOC were used in this work to derive reference ground-based IWV data. The retrieved in-situ GPS IWV data were generated at a temporal resolution of 1 h. The detailed description of ground-based water vapor retrieval is presented in Section III. GPS retrieved IWV data between June 1, 2019 and May 31, 2020 from 214 GPS sites over Mainland China were employed to assess the Sentinel-3 OLCI IWV data (see Table I).

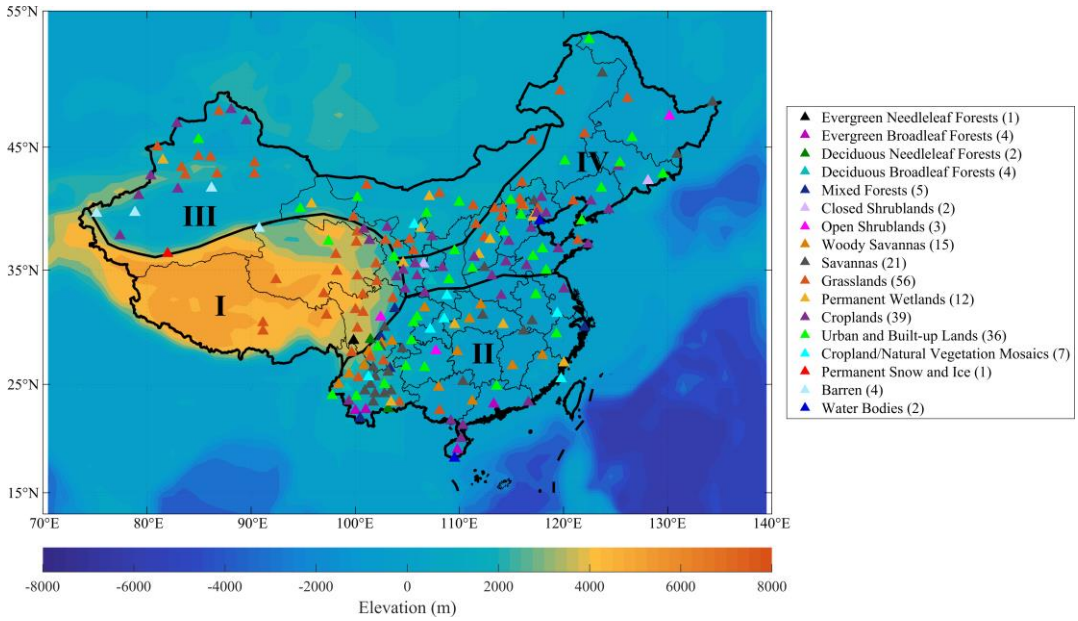


Fig. 1. Geographic distribution of the ground-based GPS sites in Mainland China. The study area is divided into four climatic zones: I. polar climate, II. temperate climate, III. arid climate, and IV. cold climate. The land cover type surrounding each GPS station is denoted with a color as shown in the legend in the right plot. The number in the parenthesis of each legend denotes the quantity of the in-situ GPS sites with the same type of land cover. The color bar represents the elevation of the GPS stations.

TABLE I
SUMMARY OF THE DATA USED IN THIS RESEARCH

| Data source | Time span | Temporal resolution | Spatial resolution | Data description |
|---|---|---|---|---|
| GPS observations | June 1, 2019 to May 31, 2020 | Hourly | 214 stations, point data | IWV estimated from GPS |
| Level-2 Sentinel-3A OLCI products | June 1, 2019 to May 31, 2020 | 4-day | 300 m | IWV estimated from Sentinel-3A |
| Level-2 Sentinel-3B OLCI products | June 1, 2019 to May 31, 2020 | 4-day | 300 m | IWV estimated from Sentinel-3B |

### *B. Satellite data*

The OLCI instrument, an imaging spectrometer evolving from the MERIS sensor on board the Envisat satellite, provides three levels of data products for the general public [41]. The Sentinel-3 OLCI Level-2 Land Full Resolution (OL_2_LFR) products [41], which include the IWV observations, are employed in this research. Two NIR channels centered at 885 nm and 900 nm of OLCI instrument are used to observe atmospheric water vapor [38]. The derived OLCI IWV data have a spatial resolution of 300 m [41]. Level-2 Sentinel-3A and Sentinel-3B OLCI IWV products acquired over the research area, were obtained from the ESA Copernicus Open Access Hub (https://scihub.copernicus.eu/dhus/#/home). All OLCI remotely sensed IWV observations from June 1, 2019 to May 31, 2020 were selected.

In the IWV evaluation, it is important to match the Sentinel-3 OLCI IWV data with the ground-based GPS-retrieved IWV data. Although geometric correction has been applied to reduce the influence of the geometric misregistration between the OLCI image pixels and the precise location of targets, this geometric misregistration problem still exists in Sentinel-3 OLCI IWV imageries [42]. Based on other studies on reducing the geometric misregistration problem in the satellite IWV evaluation [43], we utilized an OLCI IWV value averaged over the windows centering at the ground-based GPS locations. As the size of window almost has no significant effect on the satellite IWV product performance [44], the OLCI IWV data averaged over a window of 3 × 3 pixel centering at the in-situ GPS stations were taken into consideration in this study. It is required that the Sentinel-3 OLCI IWV data have at least 2 collocated data points in the 3 × 3 pixel window. By using this 3 × 3 pixel window, the geometric misregistration problem between the Sentinel-3 OLCI IWV pixel and the precise GPS location can be minimized and its effect can be reduced.

In addition, the observation time difference between the GPS IWV and the averaged OLCI IWV is required to be smaller than 30 min. Furthermore, the Level-2 OLCI product file "LQSF" was utilized as a quality control parameter in our research to obtain confident clear land pixels. Only OLCI IWV pixels flagged as "LAND", i.e., under clear sky conditions, have been taken into account in the averaging calculation and comparison analysis.

## III. METHODS

### *A. Ground-based water vapor retrieval from GPS measurements*

The ground-based IWV data were derived from the measurements from each GPS site. The approach used to determine the IWV from GPS observations is briefly described in this paper, and a more thorough explanation can be found in Bevis *et al*. [45]. The main strategy of the retrieval algorithm is

to rely upon the propagation delays caused by the troposphere, called slant tropospheric delay (STD). It can be converted to the zenith tropospheric delay (ZTD) based on the mapping functions [45], [46]. The ZTD can be decomposed into two components, a zenith hydrostatic delay (ZHD) and a zenith wet delay (ZWD) [45]:

$$ZTD = ZHD + ZWD \tag{1}$$

The ZHD is due to tropospheric gases which can be calculated using the temperature and pressure at the location of the GPS sites. The surface temperature and atmospheric pressure were acquired from European Centre for Medium-range Weather Forecasts (ECMWF) [47], [48] in this study. The ZHD is defined as [45]:

$$ZHD = (2.2997 \pm 0.0024)P_s/f(\theta, H) \tag{2}$$

$$f(\theta, H) = 1 - 0.00266\cos 2\theta - 0.00028H \tag{3}$$

where $P_s$ is the atmospheric pressure, $\theta$ is the latitude, and $H$ is the height. Then, the component ZWD can be calculated using:

$$ZWD = ZTD - ZHD \tag{4}$$

The ZWD is mainly due to the atmospheric water vapor. The relationship between IWV and ZWD is linear [45]:

$$IWV = \Pi \cdot ZWD \tag{5}$$

where the *IWV* is the water vapor derived from the ground-based GPS observations, and *Π* is a constant related to the weighted temperature of the atmosphere, which can be calculated from surface temperature [49].

In this work, the fifth generation of ECMWF Reanalysis (ERA5) data [48] (surface temperature and atmospheric pressure) were utilized to calculate the coefficient Π, in addition to the ZHD. Once the ZHD and Π are obtained, ground-based IWV data can be calculated from ZTD products of the CMONOC GPS stations [39], [40]. These in-situ GPS-retrieved IWV data selected from 214 GPS stations over Mainland China were employed to validate the retrieval accuracy of the operational OLCI IWV products.

### *B. Space-based water vapor retrieval from Sentinel-3 OLCI measurements*

The Sentinel-3 OLCI utilizes two NIR channels centered at 885 nm and 900 nm for water vapor retrieval [38]. It can measure atmospheric water vapor over land and ocean [38]. The retrieval algorithm mainly relies upon the differential absorption approach [50] to relate the IWV to the measured radiance ratio between OLCI channel O19 at 885 nm and O18 at 900 nm [38]. This retrieval model is based on the assumption that a logarithmic relation exists between the absorber mass and extinction [38]. To accelerate the calculation of the model parameters, a neural network, trained with the matrix operator model (MOMO), is employed [38]. The general form of the retrieval approach is [38], [51]:

$$W = k_0 + k_1\, log(R) + k_2 log^2(R) \tag{6}$$

where *W* is the derived IWV from OLCI measurements, and $k_0$, $k_1$, and $k_2$ are regression coefficients, and *R* is the ratio of the radiance measured in OLCI channel 19 to that of channel 18.

### *C. Statistical analysis*

In order to quantitatively validate the accuracies of the operational Sentinel-3 OLCI IWV products, OLCI IWV data were compared with in-situ GPS IWV data on an averaged pixel basis. A window of 3 × 3 pixels was averaged to get the "averaged pixel" for OLCI IWV data. Only cloud-free pixels were selected for accuracy assessment in this research. For the comparison results, the statistical parameters used in this paper include correlation coefficient ($R^2$), RMSE, mean bias (MB), and relative bias (RB). The coefficient of determination ($R^2$) provides information of the relationship strength between paired Sentinel-3 and GPS water vapor datasets. It is determined as follows:

$$R^2 = \left[\frac{\sum_{i=1}^{N}(IWV_R - \overline{IWV}_R)(IWV_O - \overline{IWV}_O)}{\sqrt{\sum_{i=1}^{N}(IWV_R - \overline{IWV}_R)^2(IWV_O - \overline{IWV}_O)^2}}\right]^2 \tag{7}$$

where *N* is the number of data pairs, $\overline{IWV}_R$ is the mean IWV from references, i.e., GPS IWV data, and $\overline{IWV}_O$ is the mean value of observations, i.e., OLCI-retrieved IWV data. The RMSE is utilized to calculate the closeness between satellite remotely sensed IWV and reference GPS-observed IWV, defined as follows:

$$RMSE = \sqrt{\frac{1}{N}\sum_{i=1}^{N}(IWV_R - IWV_O)^2} \tag{8}$$

where $IWV_R$ and $IWV_O$ have been defined above. The MB and RB provide information about the overestimation or underestimation of the Sentinel-3 OLCI IWV products by comparing with ground-based GPS derived IWV data, written as:

$$MB = \frac{1}{N}\sum_{i=1}^{N}(IWV_O - IWV_R) \tag{9}$$

$$RB = \frac{MB}{\overline{IWV}_R} \tag{10}$$

In addition, water vapor scatterplots of the operational OLCI IWV products versus reference GPS IWV data were plotted to illustrate the accuracy of official Level-2 OLCI IWV data published by Sentinel-3. The linear regression results between them were also plotted.

## IV. RESULTS

### *A. General analysis*

An overall statistical analysis between Sentinel-3 OLCI derived IWV data and GPS-measured IWV data was performed, with results shown in Fig. 2. Only spatio-temporally collocated GPS-OLCI IWV data were used in the statistical analysis. The evaluation results show that the annual RMSE values under cloud-free conditions were 3.03 mm and 3.13 mm for Sentinel-3A and Sentinel-3B, respectively. As shown in Fig. 2, the slope and intercept of the regression lines for the in-situ GPS IWV estimations versus Sentinel-3A OLCI IWV products were 1.11 and -1.41, whereas the slope and intercept for

Sentinel-3B OLCI IWV were 1.12 and -1.57. The MB and RB values for Sentinel-3 OLCI IWV data were positive. It implied that the OLCI products derived from both Sentinel-3A and Sentinel-3B measurements overestimated the IWV compared to the ground-based GPS IWV data.

Daily averaged IWV values estimated from GPS, Sentinel-3A, and Sentinel-3B are displayed in Fig. 3. These averaged IWV data were calculated from spatio-temporally collocated GPS-OLCI data sets on a daily basis. It is clearly found that the variation trend of both OLCI daily mean IWV agrees well with the GPS-retrieved daily averaged IWV. Their main difference is that the Sentinel-3A derived IWV tends to underestimate the value while the Sentinel-3B IWV tends to overestimate it. The Sentinel-3 OLCI IWV products have a good agreement with the ground-based GPS-measured daily mean IWV data, with RMSE values of 2.15 mm for Sentinel-3A and 2.26 mm for Sentinel-3B. It should be noted that, the daily averaged IWV is well associated with the characteristics of different seasons. The IWV has the largest value in summer while in winter it has the lowest value.

Since the accuracy of retrieved water vapor is closely related to the locations, the annual RMSE and MB under the clear sky conditions are determined for each GPS station in this paper. Among the 214 GPS stations, only GPS sites with more than 10 collocated data points were considered in this comparison analysis. The results shown in Fig. 4 (a) and (c) illustrate that for most in-situ GPS stations, the RMSE values between Sentinel-3 OLCI IWV and in-situ GPS IWV were in the range between 1.25 mm and 3.75 mm. The lower RMSE values were situated in the Qinghai-Tibet Plateau areas, with the RMSE usually less than 1.25 mm. In addition, most ground-based GPS sites had positive MB values, implying that both Sentinel-3A and Sentinel-3B measurements overestimated atmospheric water vapor. The sites that have negative MB (underestimated) were mainly located in the northeast and southwest regions of Mainland China.

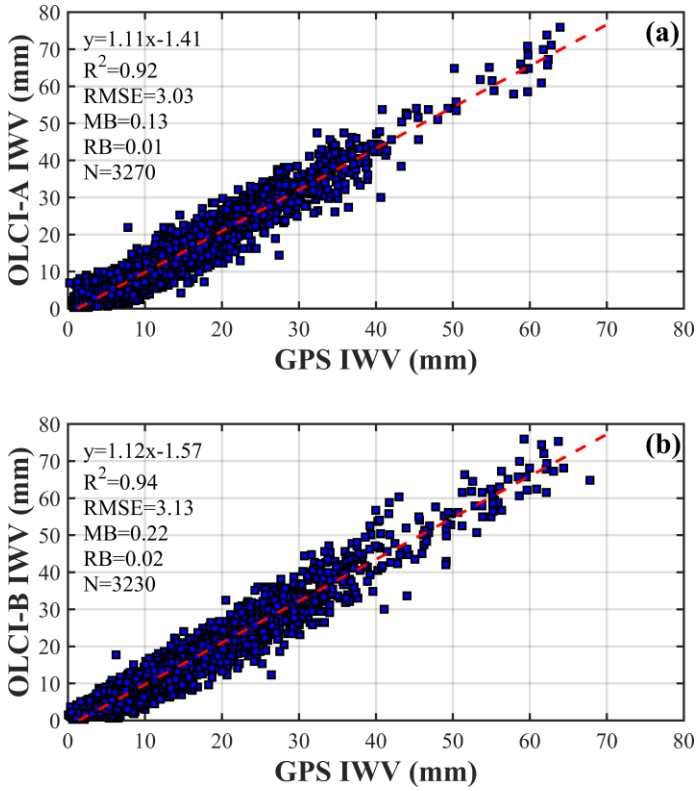


Fig. 2. Scatter plots of the ground-based GPS-derived IWV against IWV derived from (a) Sentinel-3A and (b) Sentinel-3B measurements between June 1, 2019 and May 31, 2020 in the Mainland China. N is the number of paired GPS-OLCI pixels under clear sky conditions used for evaluation. The dashed red lines show the linear regression of these data.

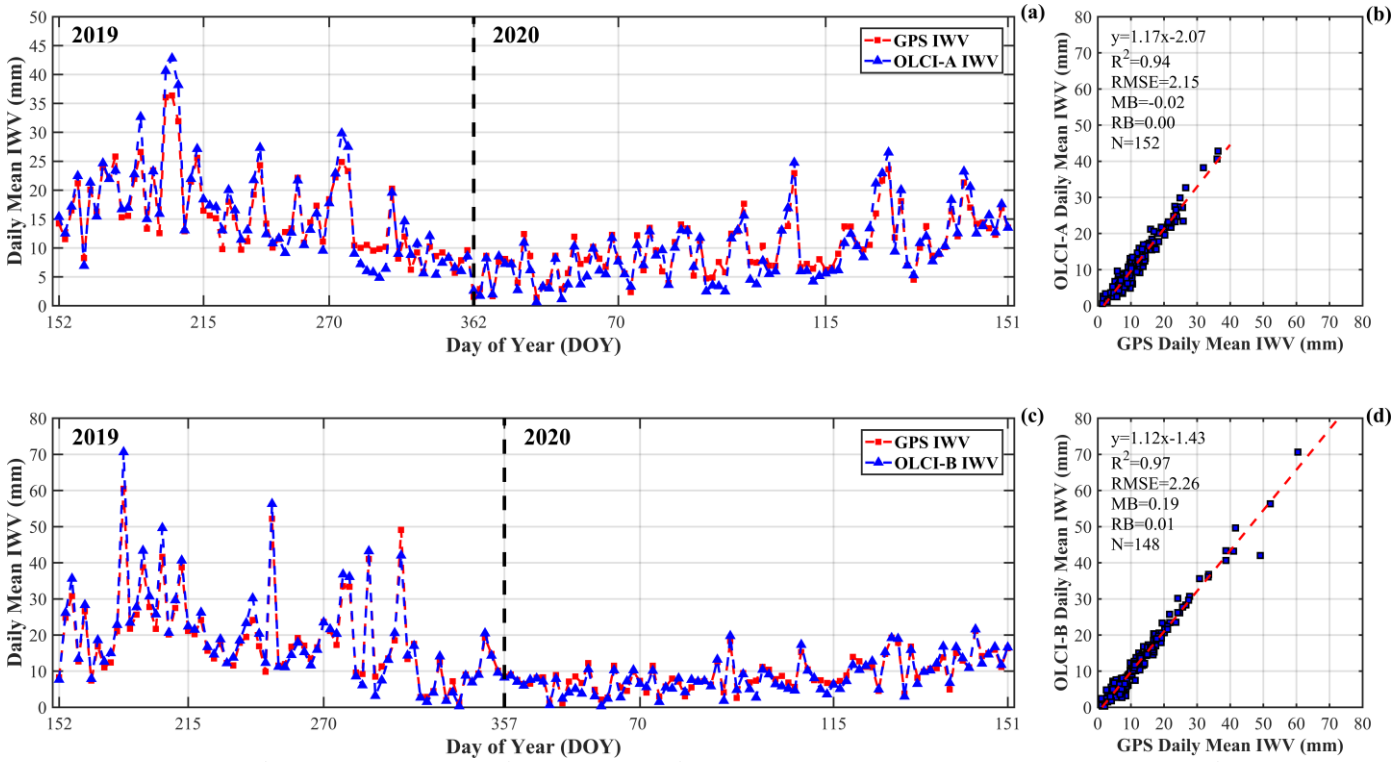


Fig. 3. Time-series analysis of daily mean IWV retrieved from observations of GPS, Sentinel-3A OLCI, and Sentinel-3B OLCI instruments from June 1, 2019 to May 31, 2020, under cloud-free conditions. (a) and (c): The daily mean variation comparison between GPS-derived daily mean IWV against Sentinel-3A and Sentinel-3B estimated daily mean IWV, respectively. (b) and (d): The scatterplots of daily mean IWV obtained from in-situ GPS observations versus Sentinel-3A and Sentinel-3B derived daily mean IWV. N is the number of paired GPS-OLCI daily averaged data under clear sky conditions used for evaluation.

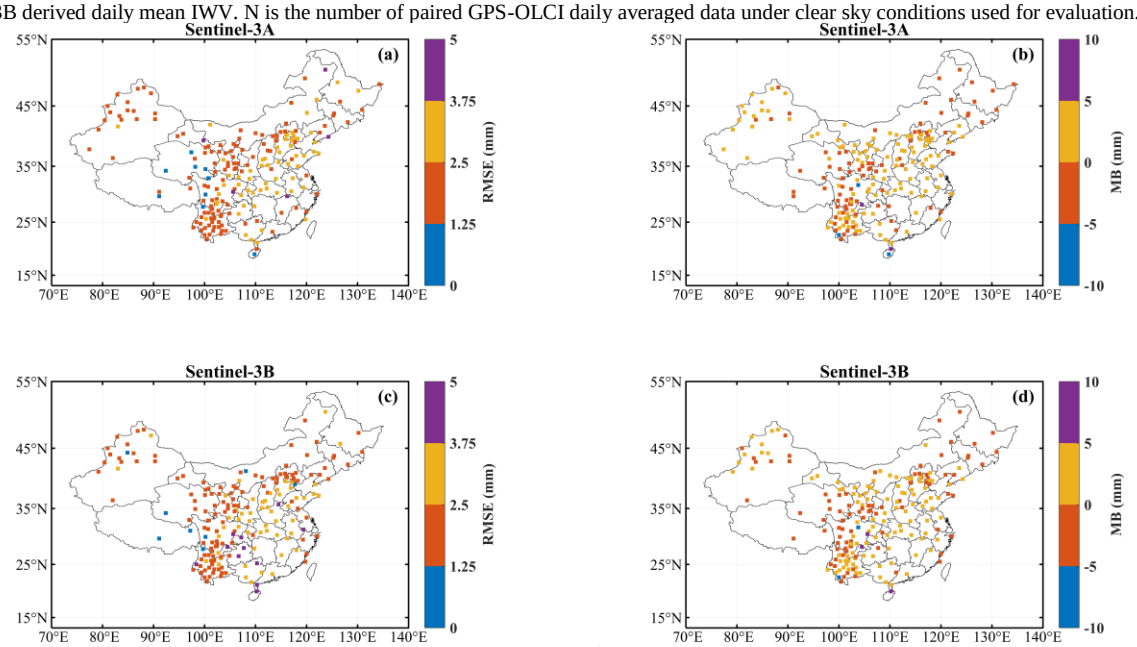


Fig. 4. Annual RMSE and MB for each ground-based GPS station during the period from June 1, 2019 to May 31, 2020 in Mainland China. (a) and (b): The RMSE and MB maps calculated from the comparison results between Sentinel-3A OLCI retrieved IWV data and GPS-observed IWV data. (c) and (d): The RMSE and MB maps calculated from the comparison results between Sentinel-3B IWV data and GPS-derived IWV data.

### *B. Analysis with inland and coastal areas*

In order to study the dependence with geographical regions, the IWV data were grouped into coastal and inland two categories. In this research, the GPS stations with a distance from the coastline less than 100 km are defined as coastal stations. The remaining GPS sites were defined as inland stations. The detailed information of the coastal GPS sites used in this evaluation analysis is listed in Table II. A total of 24 GPS stations were considered as coastal sites, while 190 GPS stations were considered as inland sites.

Fig. 5 displays the retrieval accuracy of OLCI atmospheric water vapor observations in the inland and coastal regions. It can be observed that both Sentinel-3A and Sentinel-3B retrieved IWV data have a better accuracy in the inland area

than the coastal areas. Compared with inland GPS IWV data, the RMSE were 2.96 mm and 3.04 mm for Sentinel-3A and Sentinel-3B, respectively. Compared with coastal GPS IWV data, the RMSE were 3.63 mm and 3.89 mm, respectively. The reason for this result may be that coastal stations are affected more by the oceanic humidity, which makes the IWV retrieval more challenging. In both inland and coastal areas, the Sentinel-3A IWV products show slightly better accuracy than the Sentinel-3B, with smaller RMSE (2.96 mm and 3.63 mm). In addition, the MB and RB of retrieved OLCI IWV data versus GPS-measured IWV data were all positive values for both inland and coastal stations. It indicates that the Sentinel-3 remotely sensed IWV observations are overestimated in both inland and coastal regions. It should be noted that Sentinel-3 OLCI IWV products have smaller MB and RB values in the inland area than those in coastal area. The most possible reason for this difference could be due to the effect of the oceanic humidity on the IWV retrieval.

### *C. Analysis with elevation*

The geographical elevations can also have an impact on the accuracy of atmospheric water vapor retrieval, as presented in Fig. 6. According to the elevation of classical geographical types in Mainland China, the ground-based GPS stations were divided into 5 groups based on their elevations, i.e. low plain, high plain (hill or plateau), low mountain, middle mountain, and high mountain. For these five elevation groups, the number of the paired data points is 597, 524, 839, 787, and 523 for Sentinel-3A, and 628, 508, 834, 732, and 528 for Sentinel-3B, respectively. The statistical metrics such as $R^2$, RMSE, MB, and RB were calculated for each elevation bin.

The validation results displayed in Fig. 6 indicate that, for both Sentinel-3A and Sentinel-3B, as the elevation increased, the strength of the relationship ($R^2$) between OLCI IWV and GPS IWV data decreased from 0.95 to 0.85. Similarly, the RMSE of OLCI IWV data versus GPS IWV data had lower values in higher elevation, showing the water vapor retrieval accuracy increased with the increase of elevation. The RMSE values for different elevation bins were all below 3.50 mm. Meanwhile, Sentinel-3A IWV products had positive MB and RB (overestimated) in the lower elevation (< 500 m) while in other higher elevation the MB and RB were negative (underestimated). The MB and RB values for Sentinel-3B were overall positive (overestimated), except for the elevation in the range of 2000 to around 4497 m.

TABLE II
SUMMARY OF DATA CHARACTERISTICS OF COASTAL GPS STATIONS SELECTED FOR THE INLAND AND COASTAL COMPARISON ANALYSIS

| Station | Longitude (°) | Latitude (°) | Height (m) | Location | # of pairs of data point | |
|---|---|---|---|---|---|---|
| | | | | | Sentinel-3A | Sentinel-3B |
| FJPT | 25.5 | 119.8 | 33.7 | PingTang, FuJian | 4 | 5 |
| FJXP | 26.9 | 120.0 | 80.6 | XiaPu, FuJian | 10 | 14 |
| GDST | 23.4 | 116.6 | 31.8 | ShanTou, GuangDong | 1 | 2 |
| GDZJ | 21.2 | 110.3 | 37.4 | ZanJiang, GuangDong | 11 | 12 |
| GUAN | 23.2 | 113.3 | 30.9 | GuangZhou, GuangDong | 14 | 13 |
| GXBH | 21.7 | 109.2 | 28.7 | BeiHai, GuangXi | 11 | 10 |
| GXNN | 22.6 | 108.1 | 96.8 | NanNing, GuangXi | 15 | 13 |
| HECX | 38.5 | 116.9 | 0.5 | CangXian, HeBei | 26 | 25 |
| HETS | 39.7 | 118.3 | 55.4 | TangShan, HeBei | 19 | 15 |
| HIHK | 20.0 | 110.2 | 55.2 | HaiKou, HaiNan | 6 | 3 |
| HISY | 18.2 | 109.5 | 47.0 | SanYa, HaiNan | 5 | 7 |
| JSYC | 33.4 | 120.0 | 12.7 | YanCheng, JiangSu | 10 | 7 |
| LNDD | 40.0 | 124.3 | 29.8 | DanDong, LiaoNing | 8 | 7 |
| LNHL | 40.7 | 120.9 | 42.5 | HuLuDao, LiaoNing | 14 | 16 |
| LNJZ | 39.1 | 121.7 | 67.6 | JinZhou, LiaoNing | 6 | 5 |
| LNYK | 40.7 | 122.6 | 105.6 | YingKou, LiaoNing | 17 | 18 |
| QION | 19.0 | 109.8 | 205.7 | QiongZhong, HaiNan | 2 | 1 |
| SDCY | 36.8 | 119.5 | 58.1 | ChangYi, ShanDong | 24 | 25 |
| SDRC | 37.2 | 122.4 | 64.5 | RongCheng, ShanDong | 11 | 15 |
| SDYT | 37.5 | 121.4 | 92.4 | YanTai, ShanDong | 15 | 21 |
| TJBD | 39.7 | 117.4 | -0.5 | BaoDi, TianJin | 19 | 25 |
| TJBH | 39.1 | 117.7 | -0.8 | BinHai, TianJin | 7 | 4 |
| TJWQ | 39.4 | 117.1 | 0.1 | WuQing, TianJin | 15 | 20 |
| ZJZS | 30.1 | 122.0 | 22.8 | ZhouShan, ZheJiang | 6 | 7 |

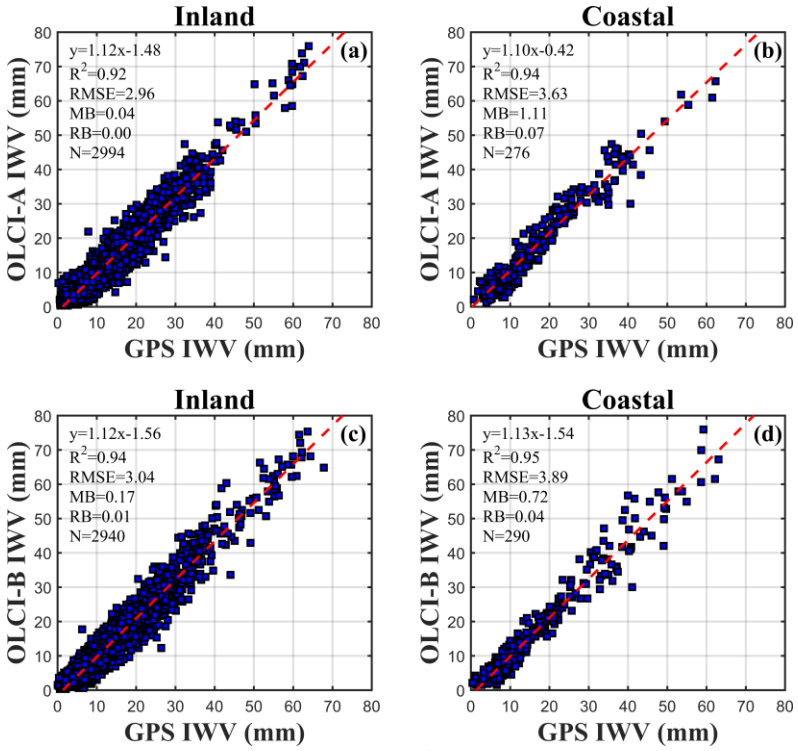


Fig. 5. Comparison between OLCI derived IWV data and GPS retrieved IWV data from June 1, 2019 to May 31, 2020 in the Mainland China. The IWV data are divided into inland and coastal two categories. (a) and (b): The scatterplots between Sentinel-3A IWV data and GPS-observed IWV data in inland and coastal areas, respectively. (c) and (d): The scatterplots between Sentinel-3B IWV data and GPS-derived IWV data in inland and coastal areas, respectively. N is the number of paired GPS-OLCI pixels under clear sky conditions used for evaluation. The dashed red lines show the linear regression of these data.

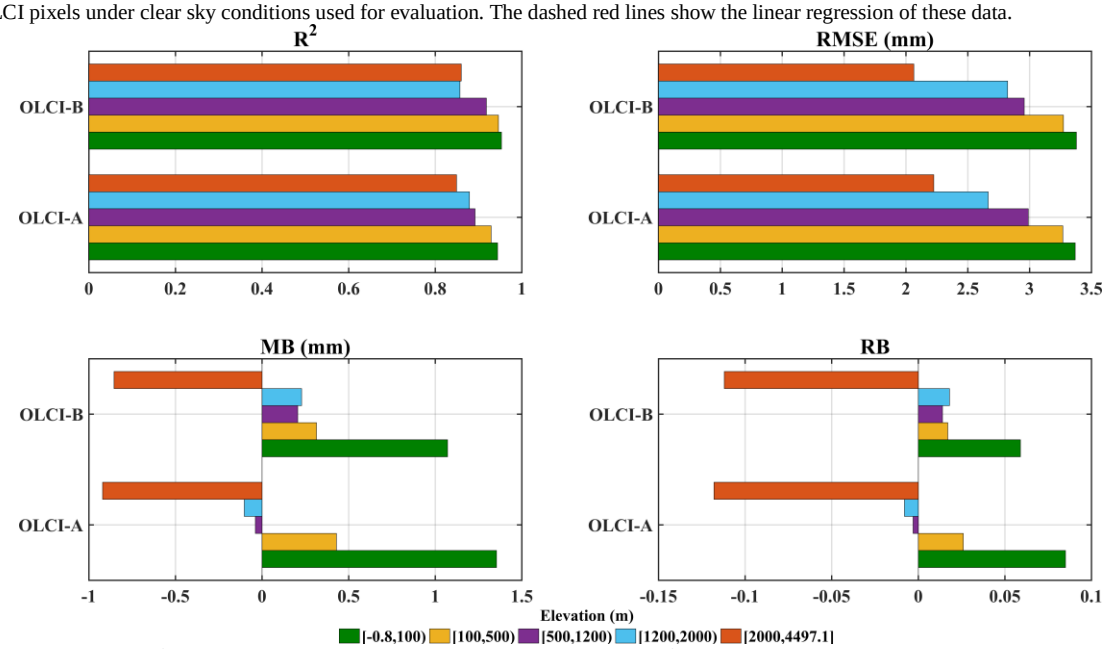


Fig. 6. The comparison analysis of OLCI-derived IWV data versus GPS-estimated IWV data for each elevation group during the period between June 1, 2019 and May 31, 2020 in the Mainland China. For each elevation group, the $R^2$, RMSE, MB, and RB are calculated. The green bar represents the elevation ranging from -0.8 to 100 m (low plain); the light yellow bar represents the elevation ranging from 100 to 500 m (high plain or hill or plateau); the purple bar represents the elevation ranging from 500 to 1200 m (low mountain); the light cyan bar represents the elevation ranging from 1200 to 2000 m (middle mountain); and the orange bar represents the elevation ranging from 2000 to 4497.1 m (high mountain).

### *D. Analysis with IWV*

IWV values can affect the performance of the satellite remotely sensed atmospheric water vapor observations. To study the IWV dependence, data were classified into three bins: low IWV (IWV < 10 mm), middle IWV (10 mm ≤ IWV < 25 mm), and large IWV (IWV ≥ 25 mm). This IWV classification is based on the previous published work on IWV analysis [32]. For low, middle, and large IWV bins, the number of the collocated data points is 1174, 1366, and 730 for Sentinel-3A, and 1106, 1304, and 820 for Sentinel-3B, respectively.

Fig. 7 shows the retrieval accuracies of Sentinel-3 OLCI IWV products for each IWV bin. It can be found that the $R^2$ and RMSE values of Sentinel-3A and Sentinel-3B behave in a very

similar trend from low IWV to large IWV. When the IWV increases, the $R^2$ and RMSE increase. That is to say that larger IWV values can result in poorer OLCI retrieval accuracies (larger RMSE). Additionally, for both Sentinel-3A and Sentinel-3B IWV products, the low IWV usually has negative MB and RB (underestimated) while the middle and large IWV usually have positive MB and RB (overestimated). However, the IWV analysis in [32] showed an opposite result, i.e. low IWV was overestimated while large IWV was underestimated. The most possible reason for this discrepancy between [32] and our research could be related to the differences in datasets, e.g. the years of observation, the areas of observation, and the number of used reference GPS stations.

### *E. Analysis with solar zenith angle*

The performance of satellite-based IWV observations can be affected by the solar zenith angle (SZA) values, which are associated with the amount of the solar radiation reflected by the Earth and atmospheric water vapor. To investigate the SZA influence on the OLCI IWV retrievals, data with SZA ranging from 20° to 70° were grouped into bins of 10° interval, including $20° \leqslant SZA < 30°$, $30° \leqslant SZA < 40°$, $40° \leqslant SZA < 50°$, $50° \leqslant SZA < 60°$, and $60° \leqslant SZA < 70°$. Corresponding to the SZA groups, the number of the collocated data points is 571, 1183, 703, 537, and 276 for Sentinel-3A, and 717, 1055, 767, 453, and 238 for Sentinel-3B, respectively.

Fig. 8 shows the accuracy of the Sentinel-3 OLCI IWV product of each SZA group. Both $R^2$ and RMSE decreased with the increase of SZA for both Sentinel-3A and Sentinel-3B satellites. That implies that larger SZA values could result in higher accuracy of the Sentinel-3 OLCI IWV product but the correlation between Sentinel-3 OLCI IWV product and GPS-estimated IWV data got worse. When the SZA was lower than 40°, Sentinel-3 OLCI IWV product tended to overestimate IWV values with positive MB and RB. When the SZA was larger than 40°, Sentinel-3 OLCI IWV product tended to underestimate IWV values with negative MB and RB. The only exception is for the Sentinel-3A OLCI IWV product with SZA in the bin of 60° to 70°, which overestimated IWV values. As reported in [32], the effect of SZA on IWV retrieval could be associated with the IWV magnitude itself. Hence, the combined effect of SZA and IWV may be responsible for Sentinel-3A's overestimation of IWV in the SZA range of 60° to 70°.

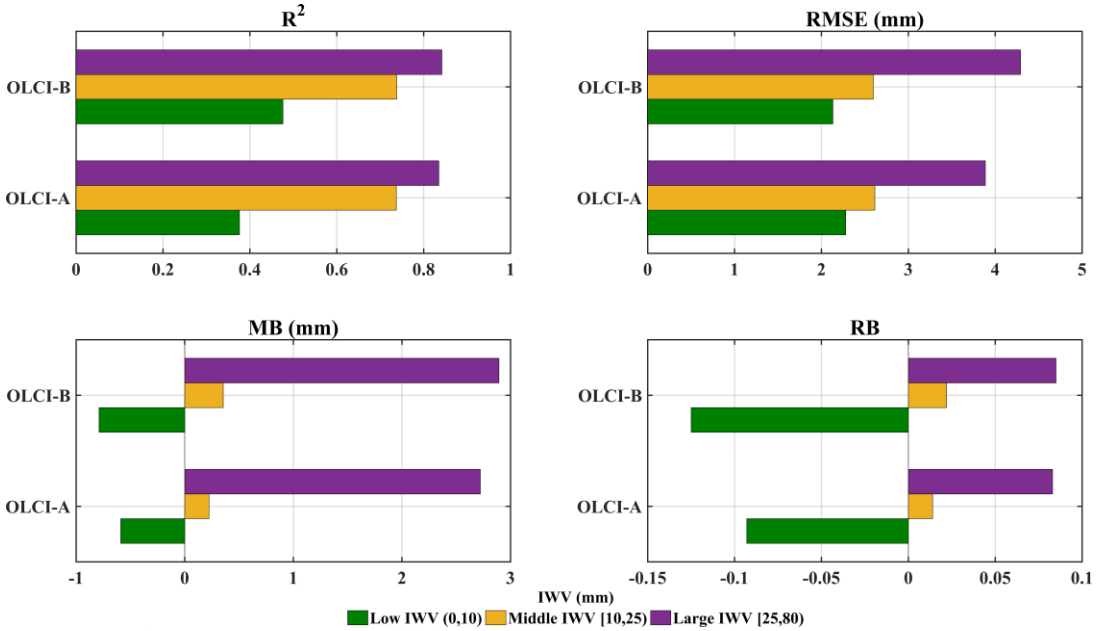


Fig. 7. The comparison analysis of OLCI-derived IWV data versus GPS-estimated IWV data for each IWV group during the period between June 1, 2019 and May 31, 2020 in the Mainland China. For each IWV group, the $R^2$, RMSE, MB, and RB are calculated. The green bar represents the IWV values ranging from 0 to 10 mm (low IWV); the light yellow bar represents the IWV values ranging from 10 to 25 mm (middle IWV); and the purple bar represents the IWV values ranging from 25 to 80 mm (large IWV).

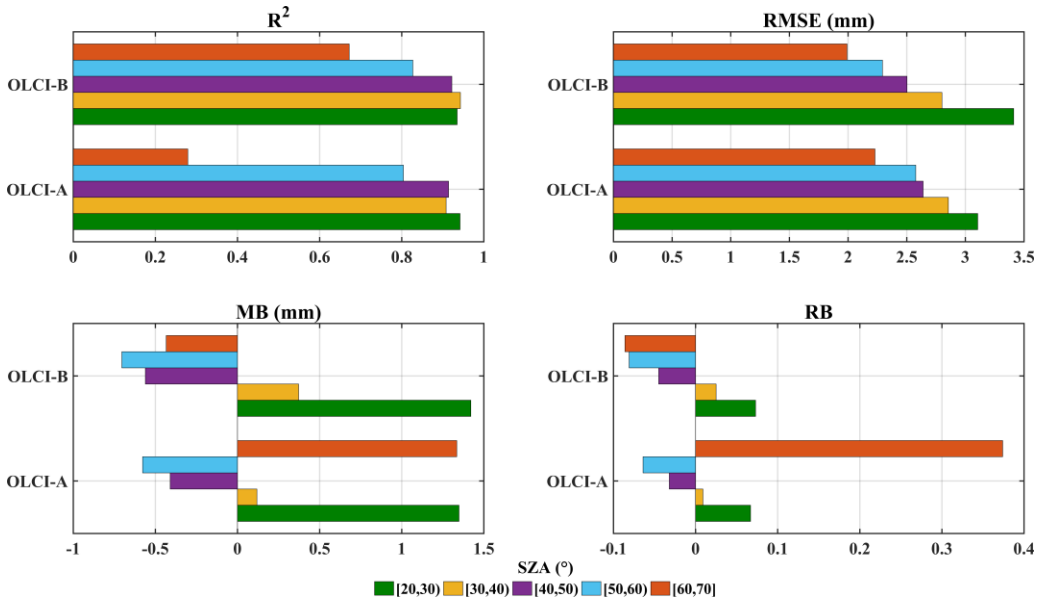


Fig. 8. The comparison analysis of OLCI-derived IWV data versus GPS-estimated IWV data for each SZA group during the period between June 1, 2019 and May 31, 2020 in the Mainland China. For each SZA group, the $R^2$, RMSE, MB, and RB are calculated. The green, light yellow, purple, light cyan, orange bars represent the SZA ranging from 20° to 30°, from 30° to 40°, from 40° to 50°, from 50° to 60°, and from 60° to 70°.

### *F. Analysis with season*

The performance of satellite measurements displays a dependence on the season of the year, because each season has its own meteorological characteristics.

In Fig. 9, the monthly $R^2$, RMSE, MB, and RB indices between OLCI IWV data and GPS measurements are shown. In general, from June 2019 to May 2020, Sentinel-3A and Sentinel-3B had similar metrics. For $R^2$, Sentinel-3A had the largest value in July 2019 and the smallest value in December 2019; Sentinel-3B had the largest $R^2$ in October 2019, with the smallest value in January 2020. From December 2019 to February 2020, the RMSE had a relatively lower value for both Sentinel-3A and Sentinel-3B IWV observations, and the relatively higher values occurred in the period between June 2019 to August 2019. In addition, there was an overall underestimation (negative MB and RB) in the months of September, December, January, February, March, and April; however, it showed an overall overestimation (positive MB and RB) in other months of OLCI IWV observations. But in the month of October 2019, the MB and RB for Sentinel-3B IWV products were negative (underestimated).

Furthermore, the seasonal dependence between Sentinel-3 OLCI IWV data and GPS IWV data are presented in Fig. 10. Data were divided into the groups of seasons: spring (March 2020 to May 2020), summer (June 2019 to August 2019), autumn (September 2019 to November 2019), and winter (December 2019 to February 2020). The number of the collocated data points in spring, summer, autumn and winter is 1436, 561, 678, and 595 for Sentinel-3A, and 1430, 662, 594, and 544 for Sentinel-3B, respectively. Seasonal evaluation results suggest that, for each season, the Sentinel-3 OLCI IWV data perform well with respect to the reference GPS IWV data. The OLCI IWV estimations showed high accuracy in spring and winter, but lower accuracy in summer and autumn, in terms of RMSE values. Moreover, it showed an overestimation (positive MB and RB) in summer and autumn for Sentinel-3A, and in summer for Sentinel-3B. In other seasons, Sentinel-3 OLCI IWV products showed an underestimated (negative MB and RB) retrieval results compared with in-situ GPS IWV data.

### *G. Analysis with land-surface-type*

The land surface type changes from location to location, which can affect the atmospheric water vapor retrieval accuracy from satellite-sensed measurements. In order to study land-surface-type dependence, data were grouped according to land cover type surrounding each GPS station (see Fig. 1). This classification was performed using MODIS annual land cover products (MCD12Q1) [52]. The International Geosphere-Biosphere Programme (IGBP) legend [52] was employed in this research. In order to obtain a more accurate surface type for each ground-based GPS site, the latest MCD12Q1 data in the year 2019 was utilized because it is the closest to the study period (June 1, 2019 to May 31, 2020). The land covers of ground-based GPS stations in Mainland China were divided into 17 classes (see Fig. 1). The validation results per land surface type are listed in Table III. The relative uncertainty was calculated as the ratio of the standard deviation to the mean from the Sentinel-3 OLCI IWV data. It shows that the Sentinel-3 OLCI IWV values used in each land cover analysis varied greatly. The $R^2$ of OLCI IWV products compared to GPS IWV data varied from 0.70 to 0.97 for Sentinel-3A satellite and from 0.83 to 1.00 for Sentinel-3B satellite. The RMSE of OLCI water vapor products were in the range of 1.66 to 3.73 mm for Sentinel-3A and 0.81 to 3.88 mm for Sentinel-3B. Table III also clearly shows that the current OLCI IWV products tend to underestimate the water vapor value in most land surface types and most land surface covers have negative MB and RB values.

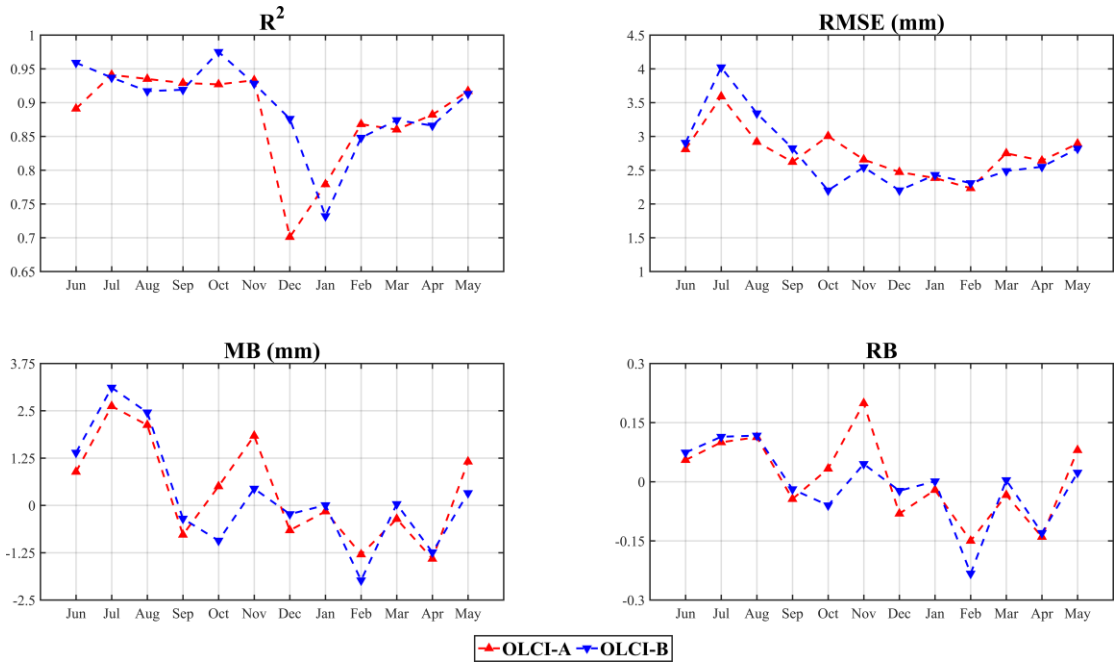


Fig. 9. The monthly comparison analysis of IWV retrieved from observations of GPS, Sentinel-3A OLCI, and Sentinel-3B OLCI instruments from June 1, 2019 to May 31, 2020 in the Mainland China. The monthly $R^2$, RMSE, MB, and RB are calculated.

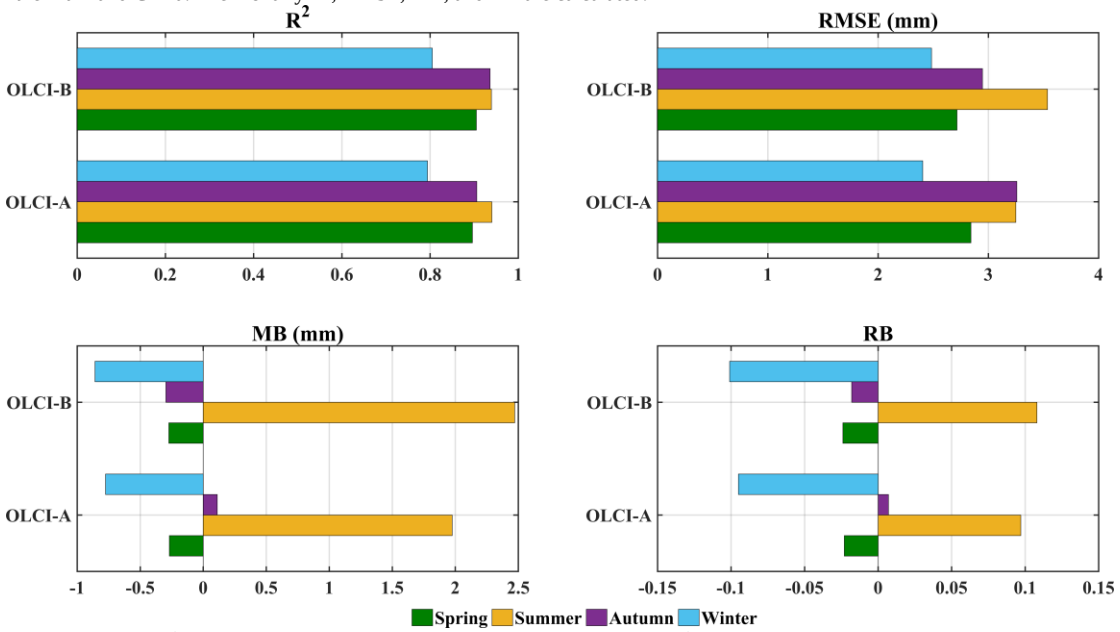


Fig. 10. The comparison analysis of OLCI-derived IWV data versus GPS-estimated IWV data for each season group during the period between June 1, 2019 and May 31, 2020 in the Mainland China. The seasonal $R^2$, RMSE, MB, and RB are calculated. The green bar represents the spring; the light yellow bar represents the summer; the purple bar represents the autumn; and the light cyan bar represents winter.

TABLE III

EVALUATION OF THE SENTINEL-3 OLCI IWV PRODUCTS AGAINST WATER VAPOR DATA DERIVED FROM THE GPS STATIONS LOCATED IN THE MAINLAND CHINA. BY EMPLOYING THE MCD12Q1 IGBP LEGEND, THE GPS STATIONS ARE DIVIDED INTO 17 CLASSES BASED ON THEIR LAND SURFACE TYPES. THE RELATIVE UNCERTAINTY IS CALCULATED AS THE RATIO BETWEEN THE STANDARD DEVIATION AGAINST THE MEAN CALCULATED FROM THE SENTINEL-3 OLCI IWV DATA

| Land cover | Satellite | # of pairs of data point | Slope | Offset | $R^2$ | RMSE | MB | RB | Relative uncertainty |
|---|---|---|---|---|---|---|---|---|---|
| Evergreen Needleleaf Forests | Sentinel-3A | 15 | 0.68 | 1.37 | 0.70 | 1.85 | -0.60 | -0.10 | 33.37% |
| | Sentinel-3B | 12 | 0.76 | 0.56 | 0.83 | 1.61 | -1.16 | -0.16 | 33.55% |
| Evergreen Broadleaf Forests | Sentinel-3A | 59 | 1.08 | -4.03 | 0.90 | 3.73 | -2.54 | -0.13 | 67.81% |
| | Sentinel-3B | 48 | 0.97 | -1.82 | 0.85 | 3.88 | -2.29 | -0.13 | 56.53% |
| Deciduous Needleleaf Forests | Sentinel-3A | 31 | 1.03 | -1.94 | 0.96 | 1.66 | -1.70 | -0.18 | 72.69% |

| | | | | | | | | | |
|---|---|---|---|---|---|---|---|---|---|
| | Sentinel-3B | 30 | 0.99 | -1.16 | 0.98 | 1.52 | -1.27 | -0.12 | 81.60% |
| Deciduous Broadleaf Forests | Sentinel-3A | 96 | 0.99 | -0.67 | 0.90 | 2.89 | -0.82 | -0.07 | 67.54% |
| | Sentinel-3B | 86 | 0.88 | 0.86 | 0.87 | 3.04 | -0.64 | -0.05 | 53.73% |
| Mixed Forests | Sentinel-3A | 61 | 1.01 | -3.36 | 0.87 | 3.70 | -3.13 | -0.19 | 74.09% |
| | Sentinel-3B | 61 | 0.98 | -2.73 | 0.93 | 3.28 | -3.02 | -0.18 | 77.65% |
| Closed Shrublands | Sentinel-3A | 40 | 0.97 | -1.60 | 0.94 | 2.15 | -1.91 | -0.18 | 71.10% |
| | Sentinel-3B | 34 | 1.01 | -1.70 | 0.94 | 2.24 | -1.55 | -0.12 | 65.40% |
| Open Shrublands | Sentinel-3A | 36 | 1.00 | -2.77 | 0.93 | 2.54 | -2.76 | -0.20 | 68.90% |
| | Sentinel-3B | 23 | 1.01 | -2.30 | 0.90 | 2.84 | -2.22 | -0.15 | 57.92% |
| Woody Savannas | Sentinel-3A | 260 | 1.13 | -2.58 | 0.96 | 2.60 | -0.44 | -0.03 | 78.48% |
| | Sentinel-3B | 240 | 1.12 | -2.57 | 0.97 | 2.91 | -0.26 | -0.01 | 78.95% |
| Savannas | Sentinel-3A | 340 | 1.13 | -1.66 | 0.93 | 2.87 | 0.27 | 0.02 | 68.24% |
| | Sentinel-3B | 297 | 1.10 | -1.33 | 0.94 | 3.05 | 0.37 | 0.02 | 72.09% |
| Grasslands | Sentinel-3A | 827 | 1.13 | -1.54 | 0.91 | 2.53 | -0.20 | -0.02 | 76.90% |
| | Sentinel-3B | 860 | 1.16 | -1.90 | 0.93 | 2.40 | -0.20 | -0.02 | 81.78% |
| Permanent Wetlands | Sentinel-3A | 189 | 1.11 | -0.89 | 0.95 | 2.68 | 0.72 | 0.05 | 73.05% |
| | Sentinel-3B | 203 | 1.06 | -0.16 | 0.94 | 2.94 | 0.84 | 0.05 | 64.07% |
| Croplands | Sentinel-3A | 740 | 1.13 | -1.04 | 0.92 | 2.98 | 0.74 | 0.06 | 74.40% |
| | Sentinel-3B | 733 | 1.17 | -1.62 | 0.94 | 2.95 | 0.83 | 0.06 | 79.72% |
| Urban and Built-up Lands | Sentinel-3A | 470 | 1.16 | -1.19 | 0.92 | 2.85 | 1.02 | 0.07 | 64.91% |
| | Sentinel-3B | 495 | 1.19 | -1.94 | 0.95 | 2.70 | 1.07 | 0.07 | 71.09% |
| Cropland/Natural Vegetation Mosaics | Sentinel-3A | 89 | 1.11 | -0.93 | 0.95 | 3.22 | 1.19 | 0.06 | 66.80% |
| | Sentinel-3B | 98 | 1.06 | -0.71 | 0.95 | 3.50 | 0.54 | 0.03 | 73.71% |
| Permanent Snow and Ice | Sentinel-3A | 8 | 1.17 | -1.67 | 0.97 | 2.08 | 0.02 | 0.00 | 62.52% |
| | Sentinel-3B | 4 | 1.01 | -2.10 | 0.96 | 2.31 | -1.96 | -0.19 | 59.21% |
| Barren | Sentinel-3A | 2 | – | – | – | – | 0.46 | 0.07 | – |
| | Sentinel-3B | 2 | – | – | – | – | 1.28 | 0.11 | – |
| Water Bodies | Sentinel-3A | 7 | 1.07 | 1.12 | 0.95 | 2.42 | 1.77 | 0.18 | 68.93% |
| | Sentinel-3B | 4 | 1.41 | -6.09 | 1.00 | 0.81 | -1.63 | -0.15 | 80.29% |

### *H. Analysis with climatic zone*

China has a large area of mountains, plateaus, and plains with large climatic variations in different regions. The vast lands result in a great variety of climates in China. In this paper, the climatic zone map developed by Feng and Du [53] was employed to define the climatic zone in China. This climatic zone distribution map was generated utilizing Köppen classification approach [53], which is a widely accepted method of climate classification [54]. As shown in Fig. 1, the research area (Mainland China) has been roughly classified into four climatic zones: region I (Tibetan Plateau) is mainly covered by the polar climate; region II (southern China) is in the coverage of temperate climate; region III (north of Tibetan Plateau and west of Inner Mongolian Plateau) is defined as arid climate; and region IV (Northeast Plain and North China Plain) has a cold climate.

*1) Climatic zone I: polar climate*

The Tibetan Plateau has a critical effect on the local climate and global hydrological cycle through both thermal and mechanical forces [55]. Fig 11 (a) and (b) show a seasonal cycle in the monthly mean IWV values in climatic zone I. The seasonal maximum mean IWV had its value 13.45 mm in the summer and seasonal minimum mean IWV was 3.45 mm in winter. The seasonal maximum mean IWV values estimated from Sentinel-3A and Sentinel-3B measurements were 16.22 mm and 15.31 mm in summer, and the seasonal minimum mean IWV values were 2.19 mm and 2.16 mm in winter, respectively. The results show that the IWV value decreased from the summer to the winter, associated with the higher evaporation of surface water vapor in the summer and the decrease in rainfall in the winter. The general evaluation results in Fig. 11 (c) and (d) illustrate that OLCI IWV agrees well with the in-situ GPS IWV observations, with the RMSE of 2.52 mm for Sentinel-3A and 2.22 mm for Sentinel-3B. Both Sentinel-3A and Sentinel-3B have negative MB and RB (underestimated) in polar climate areas. The possible reason for the negative MB and RB (underestimated) is that the region has a climatic condition with IWV values usually lower than 10

mm. This is in agreement with the conclusion displayed in the IWV analysis (i.e., Section IV. D).

*2) Climatic zone II: temperate climate*

Fig. 12 (a) and (b) show a seasonal cycle in the monthly mean IWV values from June 1, 2019 to May 31, 2020 in temperate climate regions (climatic zone II). As presented in Fig. 12 (a) and (b), the IWV values were higher in the summer than in the spring and autumn, and the IWV values were smallest in the winter. The seasonal maximum mean IWV in-situ GPS value was 40.93 mm in the summer. The seasonal minimum mean GPS IWV value was 9.55 mm in the winter. The validation results displayed in Fig. 12 (c) and (d) indicate that OLCI-derived IWV data show a good relationship with the ground-based GPS-retrieved IWV data. The RMSE between them was 3.12 mm for Sentinel-3A and 3.40 mm for Sentinel-3B. In addition, the MB and RB for both Sentinel-3A and Sentinel-3B were positive, illustrating an overestimation with ground-based GPS-sensed IWV observations. The overestimation trend may be because the region has a climatic condition with IWV values usually larger than 10 mm in this region. It is consistent with the result shown in Section IV. D (i.e., Analysis with IWV).

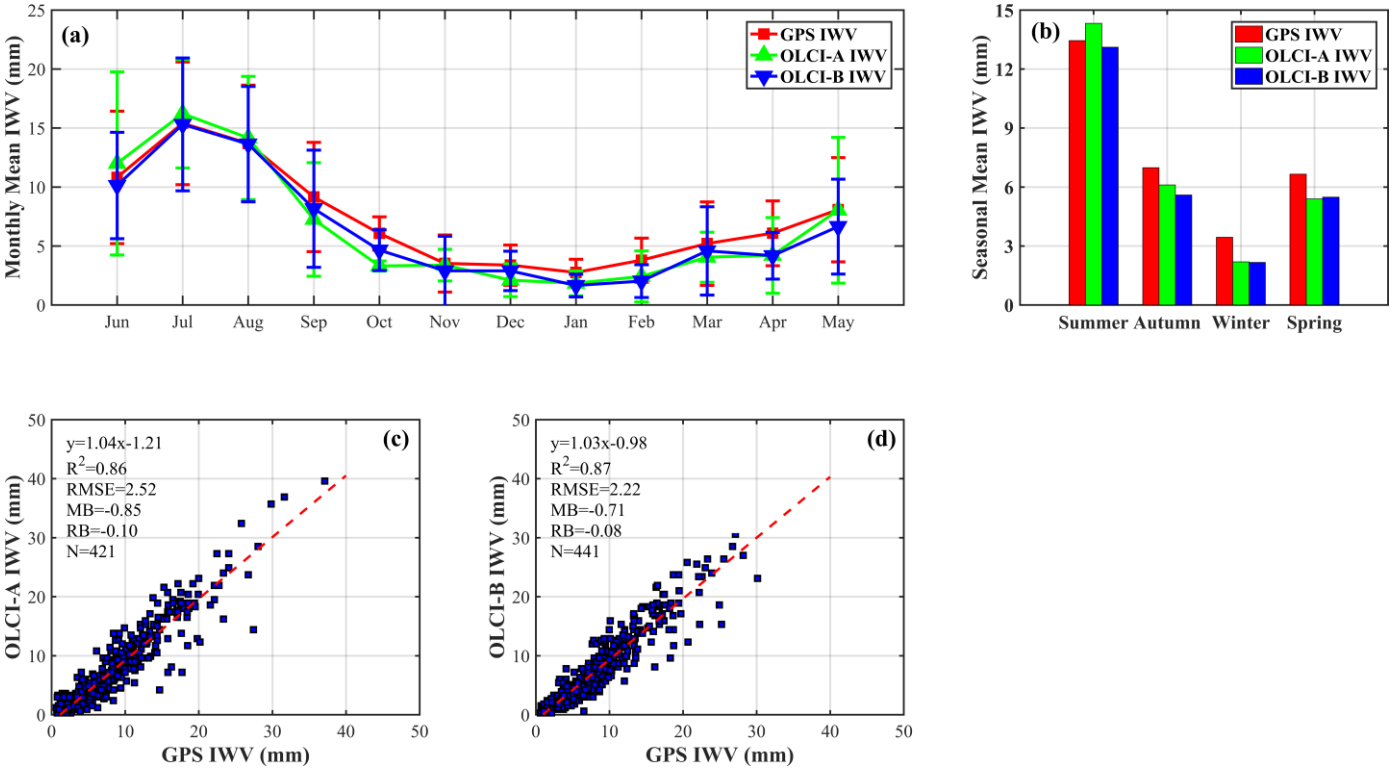


Fig. 11. The comparison analysis between Sentine-3 OLCI IWV products and GPS-observed IWV data in climatic zone I. (a) Monthly variations in IWV derived from ground-based GPS, Sentinel-3A, and Sentinel-3B measurements; error-bars in monthly averaged IWV are the standard deviation calculated from GPS, Sentinel-3A, and Sentinel-3B IWV data; (b) Variations in the seasonal mean IWV derived from ground-based GPS, Sentinel-3A, and Sentinel-3B measurements; (c) Scatterplot of the ground-based GPS IWV versus Sentinel-3A OLCI IWV; (d) Scatterplot of the ground-based GPS IWV versus Sentinel-3B OLCI IWV. N is the number of paired GPS-OLCI pixels under clear sky conditions used for evaluation.

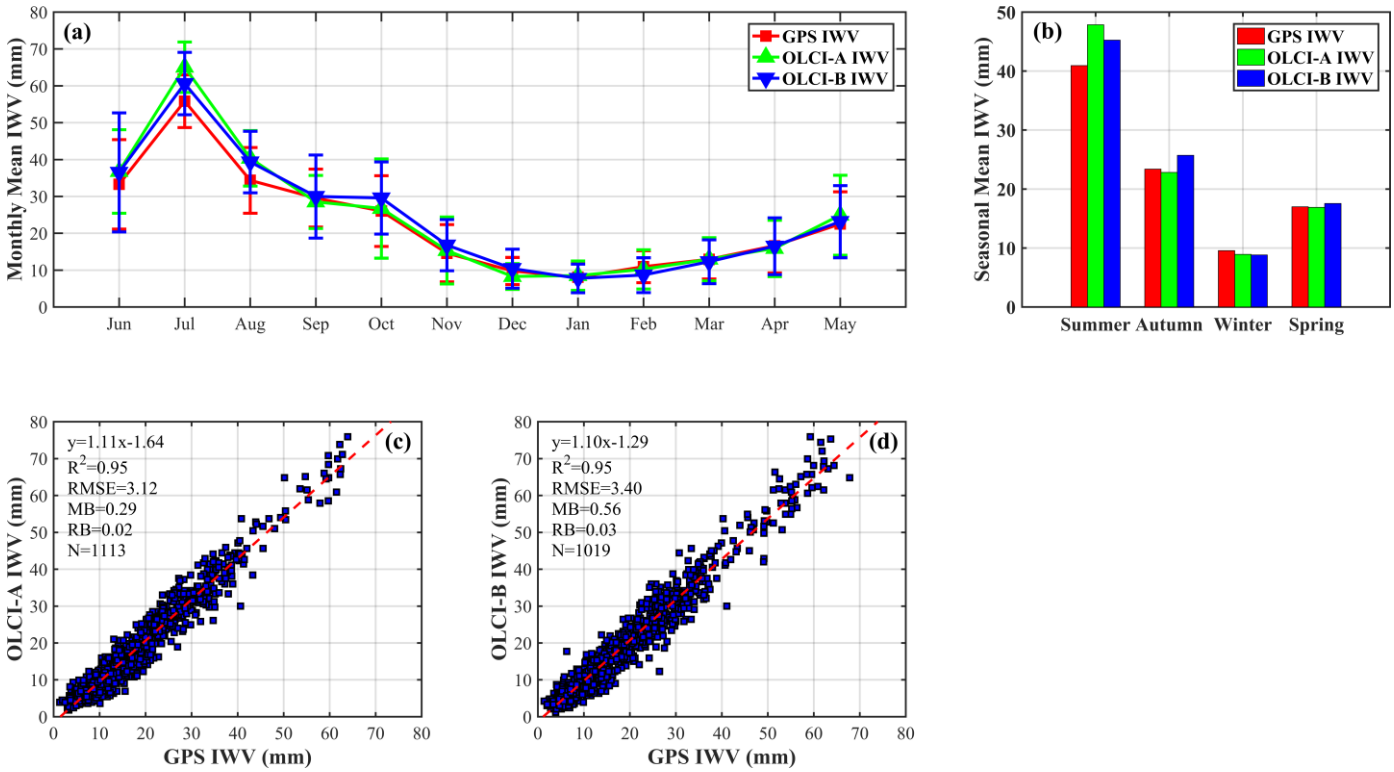


Fig. 12. The comparison analysis between Sentine-3 OLCI IWV products and GPS-observed IWV data in climatic zone II. (a) Monthly variations in IWV derived from ground-based GPS, Sentinel-3A, and Sentinel-3B measurements; error-bars in monthly averaged IWV are the standard deviation calculated from GPS, Sentinel-3A, and Sentinel-3B IWV data; (b) Variations in the seasonal mean IWV derived from ground-based GPS, Sentinel-3A, and Sentinel-3B measurements; (c) Scatterplot of the ground-based GPS IWV versus Sentinel-3A OLCI IWV; (d) Scatterplot of the ground-based GPS IWV versus Sentinel-3B OLCI IWV. N is the number of paired GPS-OLCI pixels under clear sky conditions used for evaluation.

*3) Climatic zone III: arid climate*

A regular seasonal cycle in the monthly mean IWV values in arid climate areas (climatic zone III) is displayed in Fig. 13 (a) and (b). The seasonal maximum mean GPS IWV value was 16.72 mm in the summer. The seasonal minimum mean GPS IWV value was 3.49 mm in the winter. The OLCI IWV observations exhibited larger system deviations in the summer, with the largest deviations occurring in July. The seasonal maximum mean Sentinel-3A and Sentinel-3B IWV values were 22.93 and 22.22 mm in summer, respectively, while the seasonal minimum mean values were 3.30 mm and 2.10 mm in winter. Fig. 13 (c) and (d) demonstrate that the retrieval accuracies of OLCI-sensed IWV measurements in climatic zone III is good, with the RMSE values of less than 2.60 mm (2.37 mm for Sentinel-3A and 2.55 mm for Sentinel-3B). Meanwhile, there was an overestimated (positive MB and RB) trend for both Sentinel-3A and Sentinel-3B compared with in-situ GPS IWV data. The positive MB and RB (overestimated) could be due to the middle IWV values (10 mm $\leqslant$ IWV < 25 mm) in this region, as shown in the IWV analysis (i.e., Section IV. D).

*4) Climatic zone IV: cold climate*

Fig. 14 (a) and (b) present the seasonal cycle IWV results retrieved from GPS, Sentinel-3A, and Sentinel-3B instruments in climatic zone IV, which is hot and humid in the summer (June, July, and August). The seasonal maximum mean IWV values were 24.30, 24.60, and 28.56 mm for GPS, Sentinel-3A, and Sentinel-3B, respectively. Its winter is cold and dry, with seasonal minimum mean IWV values of 5.27, 4.59, and 2.48 mm for GPS, Sentinel-3A, and Sentinel-3B, respectively. Fig. 13 (b) indicates that the OLCI measurements overestimated the IWV in the summer, whereas they underestimated the IWV in spring and winter. The evaluation results in Fig. 14 (c) and (d) show that the comparison between OLCI IWV products and GPS IWV data had a good agreement, with the RMSE values of 3.31 mm for Sentinel-3A and 3.37 mm for Sentinel-3B. The MB values of Sentinel-3A and Sentinel-3B were 0.14 mm (overestimated) and 0.06 mm (overestimated), respectively. The possible reason for the overestimation in this region is that the IWV values are usually larger than 10 mm, i.e., middle and large IWV values. It is in agreement with the result shown in Section IV. D (i.e., Analysis with IWV).

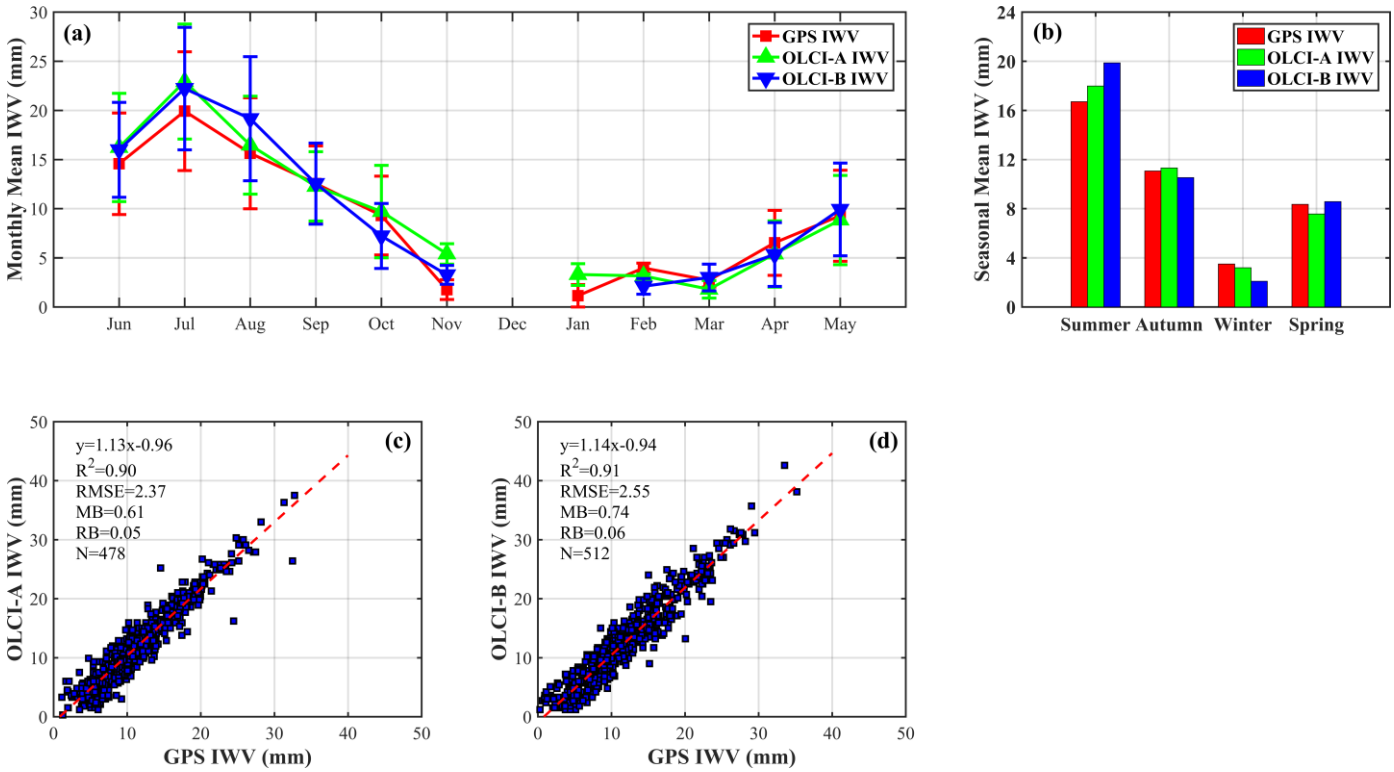


Fig. 13. The comparison analysis between Sentine-3 OLCI IWV products and GPS-observed IWV data in climatic zone III. (a) Monthly variations in IWV derived from ground-based GPS, Sentinel-3A, and Sentinel-3B measurements; error-bars in monthly averaged IWV are the standard deviation calculated from GPS, Sentinel-3A, and Sentinel-3B IWV data; (b) Variations in the seasonal mean IWV derived from ground-based GPS, Sentinel-3A, and Sentinel-3B measurements; (c) Scatterplot of the ground-based GPS IWV versus Sentinel-3A OLCI IWV; (d) Scatterplot of the ground-based GPS IWV versus Sentinel-3B OLCI IWV. N is the number of paired GPS-OLCI pixels under clear sky conditions used for evaluation.

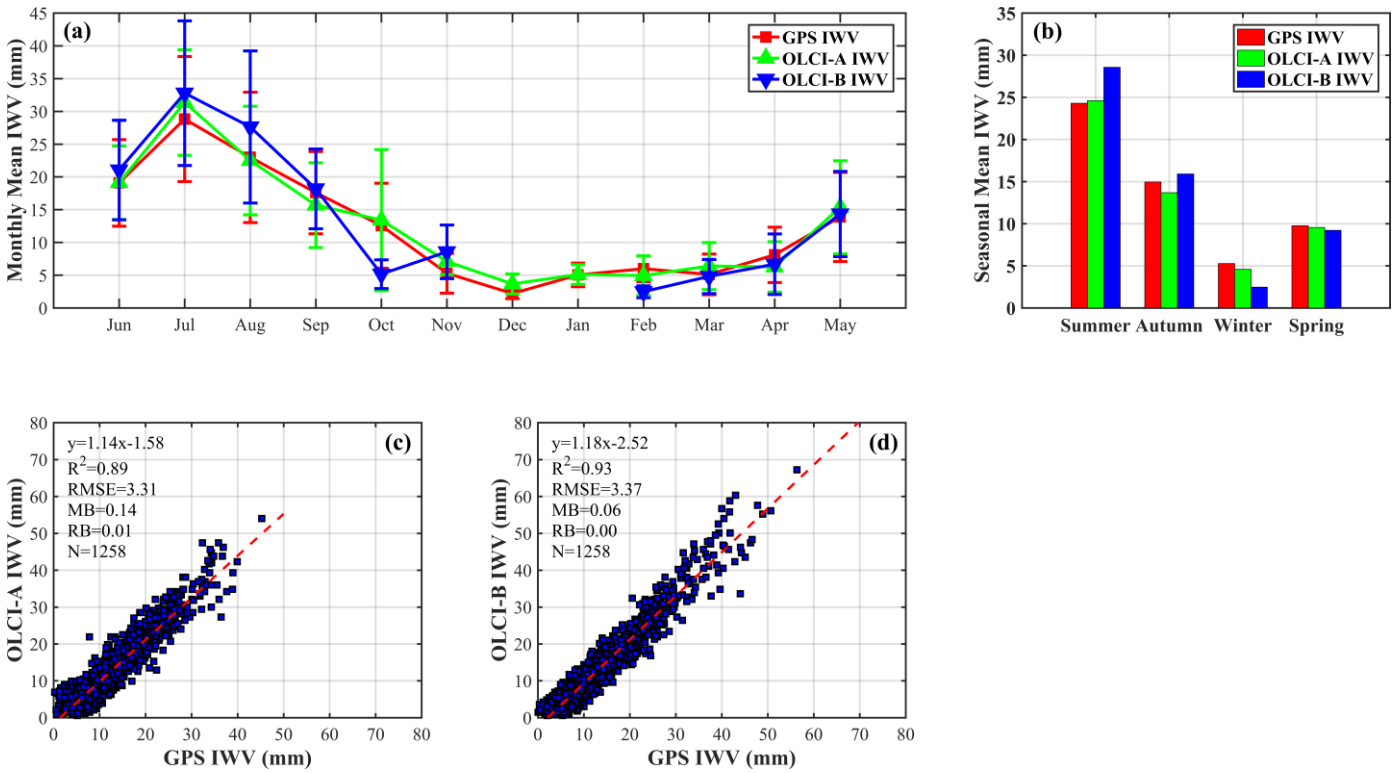


Fig. 14. The comparison analysis between Sentine-3 OLCI IWV products and GPS-observed IWV data in climatic zone IV. (a) Monthly variations in IWV derived from ground-based GPS, Sentinel-3A, and Sentinel-3B measurements; error-bars in monthly averaged IWV are the standard deviation calculated from GPS, Sentinel-3A, and Sentinel-3B IWV data; (b) Variations in the seasonal mean IWV derived from ground-based GPS, Sentinel-3A, and Sentinel-3B measurements; (c) Scatterplot of the ground-based GPS IWV versus Sentinel-3A OLCI IWV; (d) Scatterplot of the ground-based GPS IWV versus Sentinel-3B OLCI IWV. N is the number of paired GPS-OLCI pixels under clear sky conditions used for evaluation.

## V. Discussion

This study aims to validate the accuracy of Sentinel-3 OLCI IWV product by comparing against reference IWV data retrieved from ground-based GPS measurements in the Mainland China. It is the first time that the quality of Sentinel-3 OLCI IWV product is thoroughly evaluated using more than 200 in-situ GPS sites in such a large spatial coverage as China. Many variables that have an influence on the performance of Sentinel-3 OLCI IWV product have been studied. In order to have a better understanding of the results of this study, we have conducted a comparison with previous IWV evaluation studies.

### *A. Comparison with previous OLCI IWV evaluation studies*

In previous studies, comparison of Sentinel-3 OLCI IWV versus GPS IWV was carried out using regional GPS network operating mainly in Crete [35]. The MB values were -0.23 mm (underestimated) for Sentinel-3A and 0.24 mm (overestimated) for Sentinel-3B [35]. Our study showed that both Sentinel-3A and Sentinel-3B OLCI IWV products tended to overestimate IWV values, with a MB value of 0.13 mm and 0.22 mm, respectively. The MB difference of these two independent evaluations is 0.36 mm for Sentinel-3A and 0.02 mm for Sentinel-3B. In terms of relative error, it was reported that the overestimation was less than 10% compared to the regional GPS IWV data [35]. In our study, the overestimation for Sentinel-3 OLCI IWV product was not larger than 2%, with an RB value of 0.01 for Sentinel-3A and 0.02 for Sentinel-3B. The conclusion in [35] showed that OLCI instruments onboard both Sentinel-3A and Sentinel-3B satellites behaved equally well. Our validation results were in a good agreement with that.

In the official Sentinel-3 OLCI performance report provided by the Sentinel-3 Mission Performance Center (S3MPC), comparison of Sentinel-3 OLCI IWV versus GPS IWV was conducted using the SuomiNet GPS network in the North and Central America [42]. It showed that the correlation between OLCI IWV product and GPS-derived IWV data was 0.98 for Sentinel-3A and 0.97 for Sentinel-3B [42]. The RMSE of Sentinel-3A and Sentinel-3B was 2.2 mm and 2.1 mm, with the MB values of 1.24 mm and 1.02 mm, respectively [42].

In our research, the correlation between OLCI IWV product and GPS-derived IWV data was 0.92 for Sentinel-3A and 0.94 for Sentinel-3B, and the RMSE (MB) of Sentinel-3A and Sentinel-3B was 3.03 mm (0.13 mm) and 3.13 mm (0.22 mm), respectively. The conclusion shown in S3MPC performance report also suggested that the OLCI sensor of Sentinel-3A performed equally well with that of Sentinel-3B [42]. This evaluation result agreed well with our result.

Overall, our validation results are consistent with those shown in previous OLCI IWV evaluation studies.

### *B. Comparison with other satellite NIR IWV products*

The NIR channel retrieval approach has been applied in various NIR sensors to retrieve water vapor product, including OLCI, MODIS, MERSI/FY-3A, and MERIS/Envisat. He and Liu [33] evaluated the accuracy of water vapor product retrieved from MODIS/Terra, MERSI/FY-3A, and MERIS/Envisat by comparing against reference water vapor data derived from SuomiNet GPS stations in the North America. The evaluation results from this study and the [33] are summarized in Table IV.

It is clearly shown that in terms of the RMSE values, the water vapor product from both Sentinel-3A and Sentinel-3B showed a better accuracy than those from Terra, FY-3A, and Envisat. Sentinel-3A OLCI IWV product had the highest water vapor retrieval accuracy with an RMSE of only 3.03 mm, whereas the FY-3A MERSI IWV product had the lowest water vapor retrieval accuracy with an RMSE of 8.64 mm. The MB for MODIS, MERIS/Envisat, and OLCI was positive, implying that the water vapor products from these sensors tended to overestimate IWV values. The FY-3A MERSI IWV product tended to underestimate IWV values with a MB of -5.69 mm. The Terra MODIS IWV product had the best correlation with an $R^2$ of 0.95, while the water vapor product from FY-3A MERSI had the worst correlation with an $R^2$ of 0.80.

The OLCI instrument onboard the Sentinel-3 satellite is based on the proven heritage of MERIS/Envisat instrument onboard the Envisat satellite [37]. The evaluation results shown in Table IV indicated that Sentinel-3 OLCI IWV product indeed showed improved accuracy over the Envisat MERIS IWV product, with a smaller RMSE value and a lower MB value. The correlation between Sentinel-3B OLCI IWV data and GPS IWV data was slightly higher, while the Sentinel-3A OLCI IWV product was slightly lower, when compared with that of Envisat MERIS IWV product ($R^2 = 0.93$).

TABLE IV
SUMMARY OF THE VALIDATION RESULTS OF WATER VAPOR PRODUCT RETRIEVED FROM MODIS/TERRA, MERSI/FY-3A, MERIS/ENVISAT, OLCI/SENTINEL-3A, AND OLCI/SENTINEL-3B AGAINST REFERENCE WATER VAPOR DATA RETRIEVED FROM GROUND-BASED GPS MEASUREMENTS UNDER CLEAR CONDITIONS

| Sensor | Slope | Offset | $R^2$ | RMSE | MB |
|---|---|---|---|---|---|
| MODIS/Terra | 0.66 | 1.19 | 0.95 | 5.48 | 3.80 |
| MERSI/FY-3A | 1.58 | 0.55 | 0.80 | 8.64 | -5.69 |
| MERIS/Envisat | 1.49 | 0.97 | 0.93 | 3.71 | 0.95 |
| OLCI/Sentinel-3A | 1.11 | -1.41 | 0.92 | 3.03 | 0.13 |
| OLCI/Sentinel-3B | 1.12 | -1.57 | 0.94 | 3.13 | 0.22 |

## VI. Conclusion

In this study, a comprehensive comparison analysis was conducted to assess the performance of the operational Sentinel-3 OLCI IWV products against independent GPS-retrieved IWV data from June 1, 2019 to May 31, 2020 in Mainland China. For the first time, the IWV data estimated from Sentinel-3 OLCI measurements were validated using more than 200 in-situ GPS stations in a large spatial coverage. This is also the first time that the retrieval accuracies of the Sentinel-3 OLCI IWV products were evaluated against ground-based GPS-measured IWV data in China.

For Sentinel-3A and Sentinel-3B, the correlation coefficients between the OLCI IWV products and the in-situ GPS-sensed IWV measurements were $R^2 = 0.92$ and $R^2 = 0.94$, respectively, and the RMSE values were 3.03 mm and 3.13 mm, respectively. Evidently, these results indicated that the Sentinel-3 OLCI IWV measurements agree quite well with the

ground-based GPS-observed IWV data. The OLCI IWV data retrieved from Sentinel-3A have slightly higher accuracy than those estimated from Sentinel-3B. In addition, OLCI IWV data derived from both Sentinel-3A and Sentinel-3B had positive MB and RB (overestimated).

Furthermore, a detailed analysis on various parameters was also carried out. The main findings are as follows.

1) The accuracies of OLCI-derived IWV products in inland areas are superior to those in coastal areas in terms of RMSE values, due to the influence of oceanic water vapor to coastal areas.

2) When geographical elevation increases, the strength of the relationship ($R^2$) between OLCI-retrieved IWV data and GPS-observed IWV data is getting smaller; similarly, the RMSE values are likely to be smaller. Meanwhile, the MB and RB tend to be negative (underestimated) in higher elevation, but overestimated in lower elevation.

3) The larger IWV values tend to result in a lower retrieval accuracy (higher RMSE) of OLCI-observed IWV data. The MB and RB of low IWV are negative (underestimated) while the MB and RB from middle and large IWV have positive values (overestimated).

4) Larger SZA values tend to result in a higher retrieval accuracy (smaller RMSE) of the Sentinel-3 OLCI IWV product. Generally, Sentinel-3 OLCI IWV product overestimated IWV values when the SZA is lower than 40° and underestimated IWV values when the SZA is larger than 40°, except the Sentinel-3A OLCI IWV product with the SZA in the range of 60° to 70°.

5) The derived OLCI IWV data agree well with reference GPS IWV data in each season. The OLCI-retrieved IWV estimates show high accuracy in spring and winter, and lower in summer and autumn, in terms of RMSE values. It also shows an overestimated trend (positive MB and RB) in summer and autumn for Sentinel-3A IWV observations, and in summer for Sentinel-3B IWV observations.

6) For each land surface type, the RMSE of OLCI IWV data were all below 4 mm, varying from 1.66 to 3.73 mm for Sentinel-3A and from 0.81 to 3.88 mm for Sentinel-3B. The operational OLCI IWV products tend to underestimate IWV in most land cover types, as the MB and RB being negative values.

7) For each climatic zone, the maximum OLCI-retrieved IWV values occurred in the summer; the minimum OLCI-derived IWV values occurred in the winter. In addition, the IWV data retrieved from Sentinel-3A and Sentinel-3B showed a high retrieval accuracy in polar and arid climate areas, and a lower accuracy in climatic zone II and IV. It suggests that the Sentinel-3 OLCI IWV products perform better in dry areas (climatic zone I and III) than in wet areas (climatic zone II and IV). The overall MB and RB values were positive (overestimated), except for the climatic zone I (negative MB and RB, underestimated).

Comparison against previous work showed that the validation result in this study is consistent with those shown in previous OLCI IWV evaluation studies. Comparison against other satellite NIR IWV products showed that the Sentinel-3 OLCI IWV product has a superior accuracy with lower RMSE and MB values than the water vapor products retrieved from MODIS/Terra, MERSI/FY-3A, and MERIS/Envisat. It should be noted that OLCI instrument's performance in atmospheric water vapor retrieval is better than its predecessor, i.e. MERIS.

In summary, the performance of Sentinel-3 OLCI water vapor products have been comprehensively evaluated using 214 reference GPS water vapor data in China. It is expected that this study can help improve the OLCI water vapor retrieval algorithm after considering all the factors that affect OLCI IWV accuracy as shown in this work.

## ACKNOWLEDGMENT

The authors are grateful for Sentinel-3 OLCI data provided by the European Space Agency (ESA). The authors also gratefully acknowledge the support by the Crustal Movement Observation Network of China (CMONOC) for providing the GNSS-derived water vapor data used in this paper. The authors would also like to thank NASA GSFC for providing land cover products (MCD12Q1), and European Center for Medium-range Weather Forecasts (ECMWF) for providing atmospheric pressure and surface temperature data. The climatic zone map in Mainland China provided by Mr. Y. Feng from the Institute of Remote Sensing and Geographic Information System, Peking University, Beijing, China, is acknowledged.

## REFERENCES

[1] I. M. Held and B. J. Soden, "Water vapor feedback and global warming," *Annu. Rev. Energy Environ*., vol. 25, no. 1, pp. 441–475, Nov. 2000.

[2] L. Bengtsson, K. I. Hodges, S. Koumoutsaris, M. Zahn, and N. Keenlyside, "The changing atmospheric water cycle in Polar Regions in a warmer climate," *Tellus A: Dynamic Meteorology and Oceanography*, vol. 63, no. 5, pp. 907–920, Oct. 2011.

[3] M. R. Allen and W. J. Ingram, "Constraints on future changes in climate and the hydrologic cycle," *Nature*, vol. 419, no. 6903, pp. 224–232, Sep. 2002.

[4] B. J. Soden, "Global cooling after the eruption of mount Pinatubo: A test of climate feedback by water vapor," *Science*, vol. 296, no. 5568, pp. 727–730, Apr. 2002.

[5] S. Bojinski *et al*., "The concept of essential climate variables in support of climate research, applications, and policy," *Bull. Am. Meteorol. Soc.*, vol. 95, no. 9, pp. 1431–1443, Sep. 2014.

[6] Z. H. Li, J. P. Muller, and P. Cross, "Comparison of precipitable water vapor derived from radiosonde, GPS, and Moderate-Resolution Imaging Spectroradiometer measurements," *J. Geophys. Res.: Atmos.*, vol. 108, no. D20, 4651, Oct. 2003.

[7] K. E. Trenberth, J. Fasullo, and L. Smith, "Trends and variability in column-integrated atmospheric water vapor," *Climate Dyn.*, vol. 24, no. 7–8, pp. 741–758, Jun. 2005.

[8] "Implementation Plan for the Global Observing System for Climate in Support of the UNFCC." [Online]. Available: https://library.wmo.int/doc_num.php?explnum_id=3851.

[9] C. Prabhakara, H. D. Chang, and A. T. C. Chang, "Remote sensing of precipitable water over the oceans from nimbus 7 microwave measurements," *J. Appl. Meteor*., vol. 21, no. 1, pp. 59–68, Jan. 1982.

[10] M. D. King *et al.*, "Cloud and aerosol properties, precipitable water, and profiles of temperature and water vapor from MODIS," *IEEE Trans. Geosci. Remote Sens.*, vol. 41, no. 2, pp. 442–458, Feb. 2003.

[11] T. M. Scheve and C. T. Swift, "Profiling atmospheric water vapor with a K-band spectral radiometer," *IEEE Trans. Geosci. Remote Sens.*, vol. 37, no. 3, pp. 1719–1729, May. 1999.

[12] H. L. Liu *et al*., "A physical algorithm for precipitable water vapour retrieval over land using passive microwave observations," *Int. J. Remote Sens*., vol. 41, no. 16, pp. 6288–6306, Aug. 2020.

[13] "MODIS Atmospheric Profile Retrieval Algorithm Theoretical Basis Document." [Online]. Available: https://modis.gsfc.nasa.gov/data/atbd/atbd_mod07.pdf.
[14] L. Chang *et al*., "Cloud mask-related differential linear adjustment model for MODIS infrared water vapor product," *Remote Sens. Environ.*, vol. 211, pp. 650–664, Feb. 2019.
[15] Y. J. Kaufman and B. C. Gao, "Remote sensing of water vapor in the near IR from EOS/MODIS," *IEEE Trans. Geosci. Remote Sens.*, vol. 30, no. 5, pp. 871–884, Sep. 1992.
[16] R. Bennartz and J. Fischer, "Retrieval of columnar water vapour over land from backscattered solar radiation using the Medium Resolution Imaging Spectrometer," *Remote Sens. Environ.*, vol. 78, no. 3, pp. 274–283, Dec. 2001.
[17] B. C. Gao and Y. J. Kaufman, "Water vapor retrievals using moderate resolution Imaging spectroradiometer (MODIS) near-infrared channels," *J. Geophys. Res.: Atmos.*, vol. 108, no. D13, 4839, Jul. 2003.
[18] R. Lang, J. E. Williams, W. J. van der Zande, and A. N. Maurellis, "Application of the Spectral Structure Parameterization technique: retrieval of total water vapor columns from GOME," *Atmos. Chem. Phys.*, vol. 3, pp. 145–160, Feb. 2003.
[19] H. Wang, X. Liu, K. Chance, G. G. Abad, and C. C. Miller., "Water vapor retrieval from OMI visible spectra," *Atmos. Meas. Tech.*, vol. 7, no. 6, pp. 1901–1913, Jun. 2014.
[20] F. Solheim *et al*., "Radiometric profiling of temperature, water vapor and cloud liquid water using various inversion methods," *Radio. Sci.*, vol. 33, no. 2, pp. 393–404, Mar-Apr. 1998.
[21] D. D. Turner *et al*., "Retrieving liquid water path and precipitable water vapor from the atmospheric radiation measurement (ARM) microwave radiometers," *IEEE Trans. Geosci. Remote Sens.*, vol. 45, no. 11, pp. 3680–3690, Nov. 2007.
[22] R. Ohtani and I. Naito, "Comparisons of GPS-derived precipitable water vapors with radiosonde observations in Japan," *J. Geophys. Res.: Atmos.*, vol. 105, no. D22, pp. 26917–26929, Nov. 2000.
[23] A. du Piesanie *et al*., "Validation of two independent retrievals of SCIAMACHY water vapour columns using radiosonde data," *Atmos. Meas. Tech.*, vol. 6, no. 10, pp. 2925–2940, Oct. 2013.
[24] B. N. Holben *et al*., "AERONET - A federated instrument network and data archive for aerosol characterization," *Remote Sens. Environ.*, vol. 66, no. 1, pp. 1–16, Oct. 1998.
[25] C. Ichoku *et al*., "Analysis of the performance characteristics of the five-channel Microtops II Sun photometer for measuring aerosol optical thickness and precipitable water vapor," *J. Geophys. Res.: Atmos.*, vol. 107, no. D13, 4179, Jul. 2002.
[26] J. M. Dow, R. E. Neilan, and C. Rizos, "The international GNSS service in a changing landscape of global navigation satellite systems," *J. Geod.*, vol. 83, no. 3–4, pp. 191–198, Mar. 2009.
[27] X. X. Li *et al*., "Accuracy and reliability of multi-GNSS real-time precise positioning: GPS, GLONASS, BeiDou, and Galileo," *J. Geod.*, vol. 89, no. 6, pp. 607–635, Jun. 2015.
[28] H. X. Zhang, Y. B. Yuan, W. Li, and B. C. Zhang, "A real-time precipitable water vapor monitoring system using the national GNSS network of China: method and preliminary results," *IEEE J. Sel. Topics Appl. Earth Observ. Remote Sens.*, vol. 12, no. 5, pp. 1587–1598, May. 2019.
[29] O. Bock, C. Keil, E. Richard, C. Flamant, and M. N. Bouin, "Validation of precipitable water from ECMWF model analyses with GPS and radiosonde data during the MAP SOP," *Q. J. R. Meteorol. Soc.*, vol. 131, no. 612, pp. 3013–3036, Oct. 2005.
[30] A. K. Prasad and R. P. Singh, "Validation of MODIS Terra, AIRS, NCEP/DOE AMIP-II Reanalysis-2, and AERONET Sun photometer derived integrated precipitable water vapor using ground-based GPS receivers over India," *J. Geophys. Res.: Atmos.*, vol. 114, D05107, Mar. 2009.
[31] M. Shangguan *et al*., "A global assessment of NASA AIRS v6 and EUMETSAT IASI v6 precipitable water vapor using ground-based GPS SuomiNet stations," *J. Geophys. Res.: Atmos.*, vol. 121, no. 15, pp. 8925–8948, May. 2016.
[32] J. Vaquero-Martinez *et al*., "Inter-comparison of integrated water vapor from satellite instruments using reference GPS data at the Iberian Peninsula," *Remote Sens. Environ.*, vol. 204, pp. 729–740, Jan. 2018.
[33] J. He and Z. Z. Liu, "Comparison of satellite-derived precipitable water vapor through near-infrared remote sensing channels," *IEEE Trans. Geosci. Remote Sens.*, vol. 57, no. 12, pp. 10252–10262, Dec. 2019.
[34] H. Q. Wang, A. H. Souri, G. G. Abad, X. Liu, and K. Chance, "Ozone Monitoring Instrument (OMI) total column water vapor version 4 validation and applications," *Atmos. Meas. Tech.*, vol. 12, no. 9, pp. 5183–5199, Sep. 2019.
[35] S. Mertikas *et al*., "Validation of Sentinel-3 OLCI integrated water vapor products using regional GNSS measurements in Crete, Greece," *Remote Sens.*, vol. 12, no. 16, 2606, Aug. 2020.
[36] C. Donlon *et al*., "The Global Monitoring for Environment and Security (GMES) Sentinel-3 mission," *Remote Sens. Environ.*, vol. 120, pp. 37–57, May. 2012.
[37] N. Lamquin, S. Clerc, L. Bourg, and C. Donlon, "OLCI A/B tandem phase analysis, part 1: Level 1 homogenisation and harmonisation," *Remote Sens.*, vol. 12, no. 11, 1804, Jun. 2020.
[38] "Retrieval of Total Water Vapour Content from OLCI Measurements." [Online]. Available: https://earth.esa.int/documents/247904/349589/OLCI_L2_ATBD_Water_Vapour.pdf.
[39] Q. Wang, and P. Zhang, "The initial result of crust movement observation network of China: GPS-derived velocity field (1998–2001)," *AGU Fall Meeting*, 2001.
[40] Q. M. Chen *et al*., "Assessment of ZTD derived from ECMWF/NCEP data with GPS ZTD over China," *GPS Solut*., vol. 15, no. 4, pp. 415–425, Oct. 2011.
[41] "Sentinel-3: ESA's Global Land and Ocean Mission for GMES Operational Services." [Online]. Available: https://sentinels.copernicus.eu/documents/247904/351187/S3_SP-1322_3.pdf.
[42] "Sentinel-3 Data Product Quality Reports." [Online]. Available: https://sentinels.copernicus.eu/documents/247904/4069162/Sentinel-3-MPC-ACR-OLCI-Cyclic-Report-056-037.pdf.
[43] F. L. Shi *et al*., "The first validation of the precipitable water vapor of multisensor satellites over the typical regions in China," *Remote Sens. Environ*., vol. 206, pp. 107–122, Mar. 2018.
[44] J. Vaquero-Martinez *et al*., "Water vapor satellite products in the European Arctic: An inter-comparison against GNSS data," *Sci. Total Environ*., vol. 741, Nov. 2020.
[45] M. Bevis *et al*., "GPS meteorology-remote sensing of atmospheric water vapor using the global positioning system," *J. Geophys. Res.: Atmos.*, vol. 97, no. D14, pp. 15787–15801, Oct. 1992.
[46] T. Ning *et al*., "The uncertainty of the atmospheric integrated water vapour estimated from GNSS observations," *Atmos. Meas. Tech.*, vol. 9, no. 1, pp. 79–92, Jan. 2016.
[47] L. Hoffmann *et al*., "From ERA-Interim to ERA5: the considerable impact of ECMWF's next-generation reanalysis on Lagrangian transport simulations," *Atmos. Chem. Phys.*, vol. 19, no. 5, pp. 3097–3124, Mar. 2019.
[48] H. Hersbach *et al*., "The ERA5 global reanalysis," *Q. J. R. Meteorol. Soc.*, vol. 146, no. 730, pp. 1999–2049, Jul. 2020.
[49] X. M. Wang, K. F. Zhang, S. Q. Wu, S. J. Fan, and Y. Y. Cheng, "Water vapor-weighted mean temperature and its impact on the determination of precipitable water vapor and its linear trend," *J. Geophys. Res.: Atmos.*, vol. 121, no. 2, pp. 833–852, Jan. 2016.
[50] D. Schläpfer, C. C. Borel, J. Keller, and K. I. Itten, "Atmospheric precorrected differential absorption technique to retrieve columnar water vapor," *Remote Sens. Environ.*, vol. 65, no. 3, pp. 353–366, Sep. 1998.
[51] R. Bennartz and J. Fischer, "Retrieval of columnar water vapour over land from backscattered solar radiation using the Medium Resolution Imaging Spectrometer," *Remote Sens. Environ.*, vol. 78, no. 3, pp. 274–283, Dec. 2001.
[52] "User Guide to Collection 6 MODIS Land Cover (MCD12Q1 and MCD12C1) Product." [Online]. Available: https://lpdaac.usgs.gov/documents/101/MCD12_User_Guide_V6.pdf.
[53] Y. Feng and S. Du, "Climate changes and landscape responses of China during the past 40 years (1979-2018) under Köppen -Geiger climate classification," *ISPRS Ann. Photogramm. Remote Sens. Spatial Inf. Sci.*, vol. V-3-2020, pp. 731–737, Aug. 2020.
[54] P. R. Larson and C. F. Lohrengel, "A new tool for climatic analysis using the Koppen climate classification," *J. Geog.*, vol. 110, no. 3, pp. 120–130, May. 2011.
[55] W. X. Zhang, T. J. Zhou, and L. X. Zhang, "Wetting and greening Tibetan Plateau in early summer in recent decades," *J. Geophys. Res.: Atmos.*, vol. 122, no. 11, pp. 5808–5822, Jun. 2017.

**Jiafei Xu** received the B.Sc. degree in remote sensing science and technology from Shandong Agricultural University,

Taian, China, in 2015, and M.Sc. degree in geomatics engineering from Aerospace Information Research Institute, Chinese Academy of Sciences (CAS), Beijing, China, in 2019. He is currently pursuing the Ph.D. degree with the Department of Land Surveying and Geo-Informatics, The Hong Kong Polytechnic University, Hong Kong.

His current research interests include the algorithm development for precipitable water vapor retrieval from multi-sensor data using ground-based GNSS measurements, and the algorithm validation for various space-sensed precipitable water vapor products by conducting comparisons with reference data, such as GNSS, radiometer, and reanalysis products.

**Zhizhao Liu** received the B.Sc. degree in Surveying Engineering from Jiangxi University of Science and Technology, Ganzhou, China, in 1994; the M.Sc. degree in Geodesy from the Wuhan University, Wuhan, China, in 1997; and the Ph.D. degree in Geomatics Engineering from the University of Calgary, Calgary, Alberta, Canada, in 2004.

He is currently a Professor with the Department of Land Surveying and Geo-Informatics, The Hong Kong Polytechnic University, Kowloon, Hong Kong, China. His research interests include new algorithm development for precise Global Positioning System (GPS) and Global Navigation Satellite System (GNSS), GPS/GNSS precise point positioning (PPP), ionosphere modeling and scintillation monitoring, tropospheric remote sensing and modeling, and GPS/GNSS meteorology. He has over 20 years of experience in GPS/GNSS research. His group developed China's first GPS PPP-based Precipitable Water Vapor Real-time Monitoring System in the Pearl-River-Delta region in 2012. His research group established Hong Kong's first GPS/GNSS-radiosonde water vapor sounding collocation system in 2013 in collaboration with Hong Kong Observatory. In 2012, his group developed Hong Kong's first GPS/GNSS-based ionosphere scintillation monitoring system (two stations deployed in South and North Hong Kong) with his collaborators.

Dr. Liu was the recipient of the inaugural Early Career Award of the Hong Kong Research Grants Council (RGC), Hong Kong, in 2012 and was the recipient of the inaugural Best Conference Paper of the China Satellite Navigation Conference (CSNC), China, in 2013. In 2014, he was nominated by the Hong Kong Observatory for the World Meteorological Organization (WMO) "Norbert Gerbier-MUMM International Award for 2015" for his paper that has developed a method to evaluate the absolute accuracy of water vapor measurements, in addition to other numerous awards and honors.